VECTOR MESON PRODUCTION IN ULTRA-PERIPHERAL COLLISIONS

A Thesis

by

JAMES O. THOMAS

Submitted to the Office of Graduate Studies
of Texas A&M University-Commerce
in partial fulfillment of the requirements
for the degree of
MASTER OF SCIENCE
May 2016

VECTOR MESON PRODUCTION IN ULTRA-PERIPHERAL COLLISIONS

A Thesis

by

JAMES O. THOMAS

Approved by:

Advisor:	Carlos Bertulani
Committee:	Bao-An Li William Newton
Head of Department:	Matt Wood
Dean of the College:	Brent Donham
Dean of Graduate Studies:	Arlene Horne

ABSTRACT

VECTOR MESON PRODUCTION IN ULTRA PERIPHERAL COLLISIONS

James O. Thomas, MS
Texas A&M University-Commerce, 2016

Advisor: Carlos Bertulani, PhD

Charged ions moving at relativistic speeds generate strong electromagnetic fields (E/M) that, at regions outside the source (important when the E/M sources are nuclei), behave like the fields from a beam of real photons. These equivalent, or virtual photons, can induce an excitation in another nucleus as the source flies by. Existing theories attempt to explain such processes and predict their outcome. One way to study such Ultra-Peripheral Collisions (UPCs) is to simulate them using a Monte-Carlo Multi-Collisional (MCMC) model based on nucleon degrees of freedom. The CRISP (acronym for Collaboration Rio-Illhéus-São Paulo) model is one such theory. It is basically at the stage of a well-documented software package that implements the MCMC. This model has successfully predicted observables, such as neutron multiplicity, from central collisions and also in UPCs with relativistic heavy ions. However, the photoproduction of vector mesons has only recently been added to the CRISP model. A completely different approach to study UPCs focuses on the role of Parton Distribution Functions (PDFs) in the excitation process. Here, instead of nucleons, the degrees of freedom are quarks and gluons

(generically known as partons). Several distinct PDFs exist in the literature and are continually being updated.

This work used experimental results released from the ALICE collaboration at the Large Hadron Collider (LHC) facility located at the international particle physics laboratory CERN in Switzerland. Our outputs from the CRISP model, and from the sub-nucleon degrees of freedom model, were photonuclear cross sections for vector meson production. A comparison of our results with the experimental data allowed us to constrain different PDFs, as well as the effect of multiple collisions on the production of mesons with nucleons in the final channel.

Upon completion of the calculations, it was seen that the hadronic models could accurately predict the production of the J/psi meson, but not the rho. It was also seen that the use of different parton distribution functions led to significantly different results in both the rapidity distributions for vector meson production as well as the total cross sections. Due to the wildly different results, it was concluded that more work is needed before either method is suitable to accurately predict experimental observables.

ACKNOWLEDGEMENTS

I would like to recognize my family and friends. Without their love and support this thesis would not have been possible. I would especially like to thank my nephew for his constant reminders that life is for living.

I am also indebted to Dr. Cathy Clewett and Dr. Todd Alam for their academic and professional guidance as I started my physics education. Their helpful suggestions have guided me along a path that would have been unattainable without their input.

I would also like to thank my professors, specifically Dr. Bertulani and Dr. Li, for presenting difficult and complex physics topics in a way that makes them attainable and understandable. For their camaraderie and humor, I am also grateful for my fellow classmates and labmates, specifically Nathan Brady.

While completing this work I had the honor of collaborating with several individuals. Evandro Segundo patiently explained the details of the CRISP models as well as the basics of using Linux and the C++ programming language. Benjamin Clark's expertise in the use of PDFs was also invaluable to me. His thoughtful comments and questions guided the section of this work regarding the parton distribution functions.

I am also grateful for the support of the Physics Department at Texas A&M University-Commerce. Their financial support throughout my time here has allowed me to pursue and attain a master's degree.

I would like to thank my thesis adviser, Dr. Carlos Bertulani, for his immense support and advice that he has given me, both in and out of the class room. Finally, I would also like to thank Dr. Li and Dr. Newton for taking time to be part of my thesis committee.

TABLE OF CONTENTS

LIST OF TABLES ix

LIST OF FIGURES x

CHAPTER

1. INTRODUCTION 1

Statement of the Problem 1

Purpose of the Study 2

Hypotheses 2

Research Questions 3

Significance of the Study 3

Method of Procedure 4

Selection of Sample 4

Collection of Data 5

Treatment of the Data 5

Definitions of Terms 5

Limitations 6

Delimitations 6

Assumptions 7

Organization of Thesis Chapters 7

2. REVIEW OF THE LITERATURE 9

Equivalent Photon Method 9

CRISP 12

Parton Distribution Functions 18

3. METHOD OF PROCEDURE 23

Design of the Study 23

Sample Selection 23

Collection of Data 24

4. PRESENTATION OF FINDINGS 25

Implementation of the Equivalent Photon Method 25

Nucleon Degrees of Freedom 25

Quark Degrees of Freedom 27

Quark Degrees of Freedom with in Medium Effects 34

Total Cross Sections 43

Separation of Coherent and Incoherent Production 46

5. CONCLUSIONS 48

Summary 48

Findings 48

Recommendations for Future Research 49

REFERENCES 51

VITA 55

LIST OF TABLES

TABLE

4.1 Total cross sections for JPsi production 43

4.2 Total cross sections for Psi(2s) production 44

4.3 Total cross sections for Upsilon production 45

LIST OF FIGURES

FIGURE

2 Schematic Representation of UPCS 10

4.1 Equivalent photon spectrum 26

4.2 Total Photoproduction of J/Psi using nucleonic degrees of freedom 26

4.3 Total Photoproduction of ρ^0 using nucleonic degrees of freedom 27

4.4 Rapidity distributions for J/Psi production at $\sqrt{s_{NN}} = 2.76$ TeV 28

4.5 Rapidity distributions for J/Psi production at $\sqrt{s_{NN}} = 5.02$ TeV 28

4.6 Rapidity distributions for psi(2S) production at $\sqrt{s_{NN}} = 2.76$ TeV 30

4.7 Rapidity distributions for psi(2S) production at $\sqrt{s_{NN}} = 5.02$ TeV 31

4.8 Rapidity distributions for Upsilon production at $\sqrt{s_{NN}} = 2.76$ TeV 32

4.9 Rapidity distributions for Upsilon production at $\sqrt{s_{NN}} = 5.02$ TeV 33

4.10 Nuclear correction factors for lead 208 33

4.11 Rapidity distributions for J/Psi production at $\sqrt{s_{NN}} = 2.76$ TeV with nuclear corrections 35

4.12 Rapidity distributions for J/Psi production at $\sqrt{s_{NN}} = 5.02$ TeV with nuclear corrections 37

4.13 Rapidity distributions for psi(2S) production at $\sqrt{s_{NN}} = 2.76$ TeV with nuclear corrections 39

4.14 Rapidity distributions for psi(2S) production at $\sqrt{s_{NN}} = 5.02$ TeV with nuclear corrections 40

4.15 Rapidity distributions for Upsilon production at $\sqrt{s_{NN}} = 2.76$ TeV with nuclear corrections 41

4.16 Rapidity distributions for Upsilon production at $\sqrt{s_{NN}} = 5.02$ TeV with nuclear corrections 42

4.17 Coherent production of J/Psi at $\sqrt{s_{NN}} = 2.76$ TeV using the MSTW09 PDF and nuclear corrections 46

Chapter 1

INTRODUCTION

In particle physics, cross sections refer to the probability, or likelihood, that for a given set of conditions, a certain outcome will occur. Cross sections are expressed in units of area. For macroscopic objects that only interact through contact forces, the cross section is simply the summed geometric cross-sectional area of the objects. However, when charged particles are involved, determining the cross sections becomes significantly more difficult due to the long range of the E/M interaction.

Statement of the Problem

To date, our understanding of what makes up matter at a fundamental level and how such matter interacts is incomplete. Many possible solutions to this fundamental question, e.g., using the standard model of particle physics, have been proposed but the limited experimental data has prevented the various theories from being thoroughly vetted.

Basic theories for the nucleus rely on using nucleons, protons, and neutrons, as fundamental units. More complicated theories rely on sub-nucleon degrees of freedom. They are based on the known fact that nucleons are built up by smaller entities called quarks and gluons (generically just called partons).

Within each broad category above, many individual theories exist. Numerous theories are built upon similar hypotheses, differing only in minor details, such as the inclusion of additional quark flavors. Since the various theories attempt to explain the same physical process, they should all make similar predictions when compared against each other. However, this is often not the case. In this research we tested two such theories.

Purpose of the Study

Vector mesons are particles consisting of a quark and anti-quark. One method to theoretically tackle the problem of vector meson production in ultra-relativistic peripheral nuclear collisions is to forget about quarks and gluons and use nucleons (and other hadrons) as basic units together with their hadronic interactions. In this approach, the nucleons and the produced mesons are treated as point particles or at least we disregard their internal structure. This method is relatively simple physically. A more physically realistic approach needs to include the physics pertaining to the complicated internal structure of nucleons, that is, that they are made of quarks and gluons. Solving the underlying theory (called Quantum Chromodynamics, QCD for short) for the interactions of quarks and gluons to describe hadronic structure from first principles is extremely difficult. Many theories adopt effective models for the quark and gluon interactions and the structures that they imply. These models often need improvements which lead to greater complexity. The purpose of this study was to predict cross sections for vector meson production in peripheral collisions with relativistic heavy ions using both hadronic and partonic models. Our predictions were compared to experimental data obtained at the LHC at CERN in order to infer the pros and cons of each of these distinct models.

Hypotheses

Multiple methods are currently being used to predict the theoretical cross sections for particle production in ultra-peripheral relativistic nuclear collisions. Due to the branched nature of the current methods, I predicted the following:

1. Calculations that utilize nucleons as fundamental particles will not accurately (as compared to the experimental data) predict cross sections for vector mesons.

2. Calculations that utilize partons as fundamental particles will be able to predict accurate cross sections for vector meson production.

Research Questions

We determined how the cross section for the production of vector mesons in UPCs is affected by several properties.

1. How do different nucleon PDFs influence the number of vector mesons produced? How do different gluon contents in different nucleon PDFs influence the number of vector mesons produced?
2. How do nuclear medium effects due to the influence of quarks and gluons within different nucleons affect the nuclear PDF and consequently the number of vector mesons produced?
3. How do different nucleon (and nuclear) PDFs with modifications in the final channel due to the collisions of the vector meson with nucleons influence the dynamics of the process?

Significance of the Study

Using the equivalent photon method to calculate properties of ultra-relativistic peripheral collisions is not new. The idea was first proposed by Enrico Fermi in 1924 (as cited in Bertulani and Baur, 1988). This idea was later applied to relativistic heavy ion collisions by Weizsacker (1934) and Williams (1934). Since then, this method has been applied to numerous situations in atomic, nuclear, and particle physics. Many of the applications of the equivalent photon method were developed by Bertulani and Baur in 1988. Since the late 1980s, applications of this method have continued to increase and are being used to help explain new advances in some areas of physics. One of the applications of the equivalent photon method is to constrain PDFs in UPCs.

Since the PDFs are continually being updated by particle physics theory groups, new calculations are needed to compare to the experimental data obtained at particle accelerators. These calculations will serve to constrain the PDFs which will lead to more precise predictions of many cross sections at colliders.

Method of Procedure

Once the various PDF data sets were collected, they were used as the starting point for our UPC calculations. All of the PDF sets used are from highly reputable particle physics groups. The data collected pertaining to the hadronic model discussed previously was collected from within the extensive CRISP software package and was analyzed in a similar fashion to the PDF data.

Selection of Sample

The work detailed here is computational and theoretical; it does not require any human participants and samples. However, the results generated were compared to experimental results obtained at accelerators, such as the LHC at CERN. The LHC is currently the world's most powerful and largest particle accelerator and CERN is the European Organization for Nuclear Research and currently has twenty one member states. The experimental results were taken from highly cited, peer reviewed journal articles published by reputable collaborations, such as the ALICE collaboration, which uses the ALICE detector, which is the largest volume particle detector that has ever been constructed. The various parton distribution functions used in this study were also taken from highly cited papers and their associated models used to generate the PDF values. The hadronic interactions were calculated using the CRISP code.

Collection of Data

Since this work was mainly computational, most of the data was self-generated. However, the PDF values used when considering the subnucleonic degrees of freedom were generated by using the computer codes associated with the journal articles. All of these codes were freely available online and the only modifications were to the interface used to generate the PDF values at the required points. The CRISP code was also used as is, and the only modifications were to the input parameters and to the data processing methods used to analyze the results. In both situations above (PDF and CRISP), the inclusion of the equivalent photon method was based on highly cited and thoroughly vetted models.

Treatment of Data

After the computational models pertaining to the equivalent photon method were written and tested, the codes were used in conjunction with the results from the PDF data sets and the CRISP code to generate data that can be directly compared to experimental data. This comparison was done by plotting the generated data as well as the experimental data which determined which of the input models matched the experimental results.

Definitions of Terms

Nucleon. Neutrons and protons, when considered collectively are referred to as nucleons. These particles exist in the nucleus of normal matter (Halliday, Resnick, & Walker, 2011).

Quark. Point-like Fermionic particle that exist inside of hadrons (Das & Ferbel, 2003).

Gluon. Particle that is exchanged between two quarks in a strong process. There are 8 different gluons (Griffiths, 2008)

Parton. Collectively quarks and gluons are referred to as partons (Thomas & Weise, 2001).

Parton Distribution Function. A function that describes the distribution of momentum fraction for a specific parton (Bettini, 2008).

Differential Cross Section. Probability per unit solid angle that an incident particle is scattered into the solid angle (Krane, 1987).

Meson. Composite particle that consists of a quark and an anti-quark (Povh, Lavelle, Rith, Scholz, & Zetsche, 2008).

Vector Meson. A meson that has a total spin of 1 and negative parity (Wong, 1998).

Rapidity. A parameter related to the velocity of a particle by $\tanh(y) = v$ where y is the rapidity and v is the velocity. This parameter is additive for successive Lorentz transformations (Gottfried, 1986).

Limitations

Due to the limited computational resources available at TAMUC, all calculations were limited to 3000 simulation events for each energy step when using the CRISP code. We also only used parton distribution functions available with software packages that allowed for PDF values to be quickly obtained.

Delimitations

As we wished to study ultra-peripheral nuclear collisions, especially how such collisions can be used to constrain parton distribution functions, we did not consider how PDFs can be used for analysis of:

1. Deep inelastic scattering (DIS).
2. Heavy quarks other than the vector mesons.
3. In the case of nuclear modifications, only lead 208 will be considered.

Assumptions

In order to test how the cross section for vector meson production depends on nucleonic and sub-nucleonic degrees of freedom it was necessary to assume the following:

1. All of the parton distribution functions were used "as is" and were assumed to be free from internal errors. Any errors found within the data files used to calculate the parton distribution functions will invalidate the results obtained from those distributions functions.
2. As with any calculations that are probabilistic in their nature, slight differences in results could occur. It is assumed that such variances are small and can safely be neglected.

Organization of Thesis Chapters

In Chapter 1, I present the problem of applying parton distribution functions and nuclear parton distribution functions to the ultra peripheral nuclear collisions to calculate the cross sections of vector mesons. In Chapter 2, I discuss the development of the equivalent photon method as it pertains to ultra-relativistic peripheral collisions. I also discuss the methods necessary to combine the equivalent photon method with the parton distribution functions as well as the statistical results obtained from the CRISP software package. I cover how the data for our study were collected and how they were used in Chapter 3. Chapter 4 covers the results obtained from including equivalent photon methods with purely hadronic interactions as well as when the internal structure of the nucleons is considered. These results were then compared with the experimental quantities and any differences are discussed. In Chapter 5 I summarize the results obtained in the previous chapters as well as all the physics contained within the results.

Furthermore, I outline any limitations or constraints that became apparent during the derivation of any results. Finally, I discuss the possibilities for future work.

Chapter 2

REVIEW OF THE LITERATURE

Equivalent Photon Method

In his early 20s, Enrico Fermi proposed an idea that is still used successfully today. This idea became what is known now as the equivalent photon method (1924) or, mostly popularly, the Weizsacker-Williams method. Fermi's idea was extended to relativistic ions by Weizsacker (1934) and Williams (1934) a decade later. Due to their contributions, the method bears their names.

When a charged particle moves, it will have magnetic fields circling it and electric fields pointing in the radial direction. As the particle's speed increases to a significant fraction of the speed of light, these electromagnetic field lines, as well as any extended particle, are Lorentz contracted in the direction of the motion. At this point the composite particle resembles a pancake with electric field lines pointing outward in the transverse plane relative to the particle's direction of motion. Schematically, this can be seen in Figure 2. At a distance sufficiently far from the moving particles, the field lines from the moving ions resemble those from a superposition real photons. Because of this similarity, the fast moving particle can be replaced by an equivalent flux of real, or nearly real, photons (Bertulani, Klein, & Nystrand, 2005).

Since there are multiple equivalent photons at each collision energy, it is necessary to convert the single photon cross-section into an effective multi-photon cross section. This is accomplished using

$$\sigma = \int \frac{n(k)}{k} \sigma^{\gamma}(k) dk$$

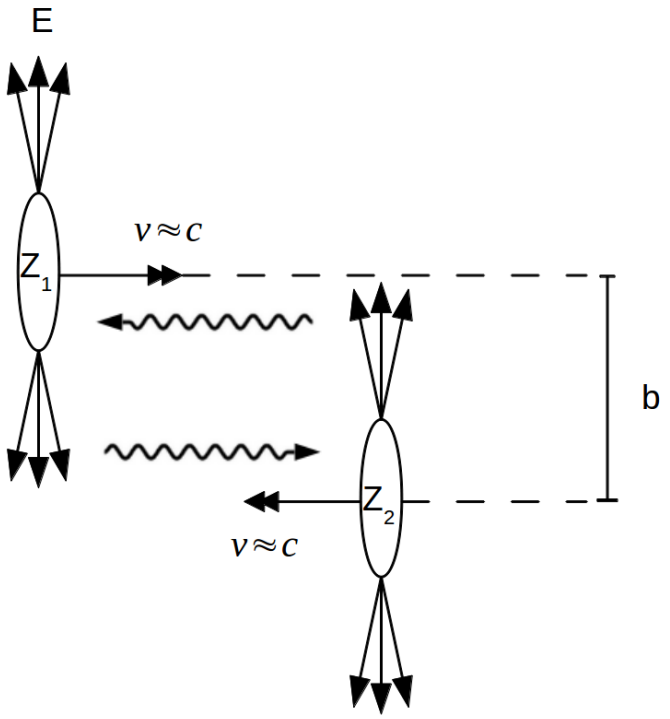

Figure 2. Comoving Lorentz contracted ions and their associated electric fields.

Where k (or ω) denotes the momentum (or energy) for a real photon, σ^{γ} is the single photon cross section, $n(k)$ is the equivalent photon flux, and σ is the effective multi-photon cross section (Bertulani et al., 2005).

The number of photons $n(k)$ can be found by taking the Fourier transform of the time dependent electro-magnetic field. Using this method the equivalent flux of photons per unit area is found to be:

$$N(k,b) = \frac{Z^2 \alpha k^2}{\pi^2 \gamma \hbar^2 \beta^2 c^2}\left(K_1^2(\zeta) + \frac{1}{\gamma^2}K_0^2(\zeta)\right)$$

where Z is the ion charge, α is the fine structure constant, γ is the Lorentz factor, βc is the particle's speed, and K_1 and K_2 are the modified Bessel functions of the second kind. $\zeta = \frac{kb}{\gamma\beta\hbar c}$ is the adiabacity parameter. The second Bessel function (K_0^2) gives the flux of photons that are longitudinally polarized and the first Bessel function (K_1^2) gives the flux of photons that are

polarized in the transverse plane (Bertulani et. al., 2005). More recent works have modified the above equation with a multiplicative factor which accounts for the survival probability of the ion: $e^{-2\,\chi(b)}$ with

$$\chi(b) = \frac{\sigma_{NN}}{4\pi}\int_0^\infty q\;\widetilde{\rho_t}(q)\widetilde{\rho_p}(q)J_0(qb)dq$$

where $\widetilde{\rho_t}(q)$ is the Fourier transform of the nuclear density of the target, $\widetilde{\rho_p}(q)$ is the Fourier transform of the nuclear density of the projectile, σ_{NN} is the total cross section of the nucleon-nucleon interaction, and J_0 is the cylindrical Bessel function of order 0 (Bertulani & Nathan, 1993). For our purposes we neglected the survival probability and instead constrained our calculations to exclude hadronic interactions by using a minimum impact parameter.

In order to find $n(k)$ we need to integrate $N(k,b)$ over impact parameter space. That is:

$$n(k) = \int N(k,b)d^2b.$$

Performing this integral yields:

$$n(k) = \frac{2Z^2\alpha}{\pi\beta^2}\left[\zeta K_0(\zeta)K_1(\zeta) - \frac{\zeta^2}{2}(K_1^2(\zeta) - K_0^2(\zeta))\right]$$

where $\zeta = \frac{kb_{min}}{\gamma\beta\hbar c}$ is the reduced adiabacity parameter. We can also express this information in terms of the derivative with respect to the photon energy:

$$\frac{dn}{dk} = \frac{2Z^2\alpha}{\pi k}\left[\zeta K_0(\zeta)K_1(\zeta) - \frac{\zeta^2}{2}(K_1^2(\zeta) - K_0^2(\zeta))\right].$$

The photon flux $\left(k\,{}^{dn}/_{dk}\right)$ from multiple colliders can be compared and is seen in publications pertaining to collider physics (Baltz et al., 2008).

CRISP

The CRISP (acronym for Collaboration Rio-Illhéus-São Paulo) is a software package developed and maintained by several leading universities in Brazil, and worldwide (Andrade-II, González, Deppman, & Bertulani, 2015; Gonzales, Guzmán, & Deppman, 2014). This software package works in several steps. First, it must build the target nucleus in the ground state. Second, a cascade of hadronic collisions is implemented with Monte-Carlo methods. This is followed by a competition between evaporation of nucleons or alpha particles and fission. We will look at these three steps in depth.

Before any calculations can be made, the program has to build the target nucleus in its fundamental, or ground, state. This is implemented using a Fermi gas model (Deppman et. al, 2004). The Fermi gas model was one of the first attempts to include some quantum mechanical effects into the methods regarding nuclear structure. For this model, the protons and neutrons are assumed to be a gas of free particles that are confined to the nuclear volume (Das and Ferbel, 2003). Within the CRISP code, each nucleon is assigned a random position inside the nuclear volume. However, the momentum of the nucleons is found in a deterministic manner using the Fermi energy.

We can relate the Fermi-momentum of a system to the Fermi-energy using

$$E_f = \frac{p_f^2}{2m}$$

where the Fermi-momentum (p_f) and the Fermi-energy (E_f) are the properties associated with the highest occupied state inside the nucleus. Using the Fermi-momentum as the maximum momentum allowed, we can calculate the volume of states in momentum space as

$$V_p = \frac{4\,\pi}{3} p_f^3.$$

We can get the volume in configuration space as

$$V = \frac{4\,\pi}{3} r_0^3 A$$

If we multiply momentum space by configuration space we get phase space. Using this on the nucleus we get:

$$V_{phase} = V_p * V$$

$$V_{phase} = \left(\frac{4\,\pi}{3}\right)^2 A\left(r_0 p_f\right)^3$$

where r_0 is an effective radius for an individual nucleon. Using the Heisenberg uncertainty principle ($\Delta x \Delta p \ \geq h$) we can assign a minimum volume in phase space that a nucleon can occupy

$$V_{min} = (2\,\pi\hbar)^3.$$

The discussion above treated protons and neutrons equally. However, this is not completely true. A more realistic treatment would necessarily have to distinguish between the two particles. With this in mind, we can state the Fermi-energy for the two different species of nucleons (Rodrigues et. al., 2004). These are given by

$$E_f^p = \frac{1}{2m_0}(3\pi)^{2/3}\ \hbar^2 \left(\frac{Z}{\Omega}\right)^{2/3}$$

$$E_f^n = \frac{1}{2m_o}(3\pi)^{2/3}\hbar^2 \left(\frac{A-Z}{\Omega}\right)^{2/3}$$

for protons and neutrons respectively. $\Omega = \frac{4}{3}\pi r_0^3 A$ is the spherical nuclear volume and m_o is the nucleon rest mass (Rodrigues et. al., 2004). Using the relativistic energy-momentum relationship, $E^2 = m^2 + \ p^2$ (where $c = \hbar = 1$) we can finally find the Fermi-momentum for the protons and neutrons.

$$p_f^p = \sqrt{E_f^p\left(E_f^p + 2m_0\right)}$$

$$p_f^n = \sqrt{E_f^n\left(E_f^n + 2m_0\right)}$$

Once the appropriate Fermi-momenta are calculated according to the above equations, the magnitudes of the momenta for the individual nucleons are uniformly distributed inside a sphere in momentum space. The neutrons are sorted from 0 to p_f^n. The protons are sorted from 0 to $p_{min}^p = p_f^n - p_f^p$. With the magnitudes of the momenta calculated in a deterministic manner, the direction of the momentum can safely be assigned randomly. Once the positions and momenta of all of the nucleons have been assigned, the nucleus is defined in its ground state. Up to this point, the interaction energy has not been considered. The interaction energy manifests itself in the equivalent photon spectrum which is considered in the next stage of this simulation.

After the nucleus has been defined in its ground state, the CRISP software package is ready to start the multi-collisional Monte-Carlo (MCMC) cascade process. The software package allows for many different projectiles to be used to initiate the cascade process, but this work focused on photon induced cascades.

For medium energies (around 40 MeV to 140 MeV) the most prevalent mechanism for photon absorption by a nucleus is thought to be the quasi-deuteron model (Rodrigues et. al., 2004). In this model, the photon is not absorbed by a single proton or a single neutron. Rather, it is collectively absorbed by a proton and a neutron behaving somewhat like a deuteron inside the larger nucleus. Within the multi-collision cascade model, the photon initially interacts with a small number of nucleons, most likely a proton and neutron. It is in these initial interactions that there is the highest probability for a vector meson to be produced. These excited nucleons then interact with more nucleons, which then, in turn, interact with even more nucleons. At each

iteration of the process, the momenta of the interacting nucleons are calculated. If the resulting momentum corresponds to a cell in momentum space that is already occupied, the interaction is disallowed. If this interaction was allowed, there would be two fermions occupying the same energy level which would violate the Pauli-exclusion principle. Thus, this blocking is aptly referred to as Pauli-blocking (Rodrigues et. al., 2004).

At each interaction step, the interaction could simply exchange momentum between the colliding particles, the collision could excite one of the interacting nucleons into a nucleonic resonance, or if there is enough energy, a vector meson could be created. If the result of an interaction is a nucleonic resonance, the CRISP software package will keep track of the position and momentum of the new particle as well as all of the remaining nucleons. Each nucleonic resonance has its own decay half life, so at each step of the cascade process the resonance could decay back down into a nucleon. The cross sections for the nucleonic resonances can be described by a Breit-Wigner formula (Deppman et. al., 2004).

$$\sigma = \sigma_0 \frac{\left(\frac{\Gamma}{2}\right)^2}{(E - E_0)^2 + \left(\frac{\Gamma}{2}\right)^2}$$

where E_0 is the mass of the resonance, Γ is the full width at half max for the resonance particle, and σ_0 is the maximum cross section associated with the particular resonance. Initially, the CRISP software package only included the Δ resonance, but the modern software includes additional heavier resonances.

If there is enough energy at a collision, there is also a possibility that a meson can be produced after the photon absorption. The current software package allows for the production of $\pi, \omega, \rho,$ and J/ψ vector mesons. Feynman diagrams for the production of and possible

subsequent decays can be seen in Figures 1 and 2 of *Nuclear photoproduction of vector mesons with Monte Carlo method* (González, Guzmám, & Deppman, 2014).

As a nucleon, resonance particle, or meson produced in the reaction approaches the edge of the nuclear volume, it has the possibility to escape from the nucleus. If the particle has enough energy to overcome the barrier used when generating the ground state for the nucleus (usually around 40 MeV) it can escape and take some of the nucleus excitation energy with it. This is where the nucleon-nucleon interaction is put into the model.

The multi-collisional cascade continues until all of the resonance particles have decayed back into nucleons and all of the particles with enough energy to escape the nucleus have done so. Once these criteria have been met, the remaining nucleus is effectively thermalized and all of the remaining excitation energy is evenly distributed among the remaining nucleons. At this point the MCMC process ends and the evaporation/fission competition can begin.

Once the multi-collisional process is completed, information about the residual nucleus is passed to the Monte-Carlo Evaporation and Fission (MCEF) package of the CRISP code. At this point it is no longer necessary for the CRISP code to keep track of individual nucleons. Instead, it is only necessary to keep track of the properties of the nucleus as a whole. The relevant properties that are kept track of include the atomic number (Z), atomic mass number (A), and the excitation energy associated with the nucleus. Currently the software package allows for neutron emission, proton emission, alpha particle emission, and fission (Deppman et.al, 2002).

At each step in the evaporation-fission process it is necessary to calculate the relative probability corresponding to the desired physical process. The probability of one particle's ejection from the nucleus relative to another particle is given by the Weisskopf's statistical model. Applying this model yields:

$$\frac{\Gamma_p}{\Gamma_n} = \left(\frac{\mathrm{E}_p^*}{\mathrm{E}_\mathrm{n}^*}\right) \exp\left\{2(a_n)^{0.5}\left[\left(r_p E_p^*\right)^{0.5} - (E_n^*)^{0.5}\right]\right\}$$

for proton emission relative to neutron emission, and

$$\frac{\Gamma_\alpha}{\Gamma_n} = \left(\frac{E_\alpha^*}{E_n^*}\right) \exp\{2(a_n)^{0.5}[(r_\alpha E_\alpha^*)^{0.5} - (E_n^*)^{0.5}]\}$$

for α emission relative to neutron emission (Deppman et. al., 2002). The probability for fission is calculated using the width derived from the liquid drop model and emission width from previous calculations. This yields:

$$\frac{\Gamma_f}{\Gamma_n} = K_f \exp\left\{2\left(a_f E_f^*\right)^{0.5} - (a_n E_n^*)^{0.5}\right\}$$

where

$$K_f = K_0 a_n \frac{2\left(a_f E_f^*\right)^{0.5} - 1}{4A^{2/3} a_f E_n^*}.$$

After calculating the probabilities for proton emission, α emission, and fission, the remaining probability must be the probability for neutron emission.

Once the necessary probabilities are calculated for the various emissions, the program generates a random number between 0 and 1 which is then compared to the above probabilities. Depending on where the random number falls, the program will select the appropriate particle emission or fission. If emission of a particle is selected, the program updates the mass number and atomic number of the remaining nucleus via:

$$A_{i+1} = A_i - \Delta\mathrm{A}_i$$

and

$$Z_{i+1} = Z_i - \Delta Z_i$$

where ΔA_i and ΔZ_i are the mass and charge number of the ejected particle respectively. The residual excitation energy is updated according to:

$$E^*_{i+1} = E^*_i - B_i - T_i$$

where B_i is the separation energy (the binding energy associated with the ejected particle while it was inside the nucleus) and T_i is the kinetic energy of the ejected particle. For neutrons $T = 2$ MeV, for protons $T = V_p$, and for α particles $T = V_\alpha$ (Deppman et. al, 2002). The residual nucleus after each iteration is then used as the initial nucleus for the next step in the MCEF process. This process continues until there is no longer enough excitation energy for particle ejection or until fission occurs.

Although the MCEF process is necessary to accurately predict many results, such as neutron multiplicity or fission rates, it is not necessary when considering vector meson production, and therefore was not used for this work.

Parton Distribution Functions

In the late 1960s, Feynman referred to the sub-particles that make up hadrons (protons and neutrons) as partons. Modern physicists classify these particles as quarks and gluons. There are six different kinds of quarks known. All of the quarks are spin ½ particles and are therefore fermions. These quarks each carry certain intrinsic properties that include, mass, electric charge, and color charge. The electric charge of the quarks is either -1/3 or +2/3 of the elementary charge unit (e). Up, charm, and top quarks all carry + (2/3)e as their electric charge. On the other hand, down, strange, and bottom quarks carry of charge of - (1/3)e. For each quark there is also an anti-quark. The anti-quark has the opposite electric charge of its corresponding quark (Griffiths, 2008).

The color charge for the quarks is described by QCD. Within QCD each quark carries one of three different colors. The term *color* here does not imply that the particles exhibit a color in the usual meaning of the word. It is simply a label that is used. The quarks always combine to

form a composite particle that is color-neutral. For this to occur, either all of the colors are present in equal amounts, or the amount of each color individually is zero. This is often referred to as color confinement. There are two rules that govern how the quarks can combine to form the particles studied in this work. First, all baryons are composed of three quarks. Therefore, every anti-baryon is composed of three antiquarks. Second, every meson is made up of a quark and an anti-quark (Griffiths, 2008). Particles consisting of more than three quarks have been proposed (Zhu, 2003), but this work focused on particles consisting of either two or three quarks.

Within particle physics, the partons are often broken up into three subcategories. First, there are three (for baryons) quarks that are referred to as valence-quarks. These valence quarks determine the quantum numbers associated with the baryon in a similar fashion to how the valence electrons determine most of the electronic properties of an atom in atomic physics. These valence quarks do not exist in isolation though. Instead they are swimming in a sea of virtual quark-antiquark pairs. The third category of partons is the gluons. It is the gluons that are responsible for holding the protons and neutrons together and they are also responsible for generating the sea of virtual quark-antiquark pairs. Collectively, the valence quarks, virtual quark-antiquark pairs, and the gluons are partons.

In order to gain information about the partonic structure of nucleons, it is necessary to use an instrument that is sensitive to very small lengths. One typical means of ascertaining such information is through deep inelastic scattering of leptons. The scattering process can be simplified if we choose the frame of reference properly. Usually the proton (or other target) is chosen to be in a system moving quickly. When this is done, the rest mass of the particles that make up the proton as well as the transverse momentum can safely be ignored. Using this set up, the structure of the target is simply given by the longitudinal momenta of all of its constituent

particles (Povh, 2008). When this is done, the interaction of the lepton can be thought of as the sum of the interactions of the constituent partons in the target. As long as the interaction between the parton and the photon is short enough that one can ignore the parton-parton interactions, this approximation works very well to reproduce experimental data.

Using the setup above, we can define a variable that is the fraction of the four-momentum of the proton that is carried by the parton that gets struck: $x = M_V^2/W_{\gamma p}$. The distributions of the momenta of all of the various partons within the nucleon are called Parton Distribution Functions (PDFs). Or, put another way, the PDFs are the probability densities of finding a parton carrying a particular momentum fraction (x) value at a particular energy scale (Q^2), where $Q^2 = -q^2$. At low energy scales most of the momentum of the nucleon is carried by the valence quarks. However, as the energy scale increases, more and more of the momentum is carried by the gluons.

One of the central tenets of modern Quantum Chromo-Dynamics (QCD) is asymptotic freedom. This means that the strength of the interaction between partons due to the strong force gets weaker and weaker as the partons get closer and closer together. At a small enough distance the interaction is arbitrarily weak (Bertulani, 2007). QCD also makes predictions about how the parton distribution functions will change with a varying energy scale. The equations that govern this process are called the DGLAP equations after Glibov and Lipatov (Gribov and Lipatov, 1972), Altarelli and Parisi (Altarelli and Parisi, 1977), and Dokshitzer (Dokshitzer, 1977). The DGLAP equations describe the interaction in the domain where pertubative calculations are valid. That is, in the limit where the strong coupling constant is much less than 1 $(\alpha_s(Q^2) \ll 1)$. Different approximations of these equations have subsequently been developed. Leading order

(LO) calculations are the most common, but next to leading order (NLO) and next to next to leading order (NNLO) are becoming more prevalent due to their increased accuracy.

The DGLAP equations do not describe how the parton distribution function changes as a function of x, they only describe how the PDFs change as a function of Q^2. Therefore, it is necessary to extract the x dependence of the PDFs from experimental data. Typically this is done by parameterizing the x dependence of the PDFs at some initial energy scale $Q^2 = Q_0^2$. The PDF can then be evolved through Q^2 space using the DGLAP equations. After this, the PDF sets are compared to experimental data, and the parameters that lead to the best fits are selected. Since the initial parameterization of x space is not defined from QCD, many different parameterizations are used. This leads to differences in PDF functions developed by different groups.

The cross section for the elastic photoproduction of vector mesons on a proton inside of a nucleus, to lowest order, is given by:

$$\sigma^{\gamma A \to VA}(k) = \zeta_V \frac{16\pi\alpha_S^2\Gamma_{ee}}{3\alpha M_V^5}\left[x g_p(x,Q^2)\right]^2 \left(\int_{t_{min}}^{\infty} |F(t)|^2 dt\right).$$

Where α is the fine structure constant, Γ_{ee} is the leptonic decay width of the vector meson being considered, α_S is the strong coupling constant which is calculated at the average momentum transfer $\bar{Q}^2 = (M_V/2)^2$, and $x = M_V^2/W_{\gamma p}^2$ is the Bjorken x. As mentioned earlier, physically x is the momentum fraction carried by the gluons. ζ_V is a correction factor that accounts for higher order terms in the PDFs, and will only be used when considering leading order PDF sets. This correction factor is described by Adeluyi and Bertulani (2011). $t_{min}(k)$ in the integral is given by $(M_V^2/4k\gamma_L)^2$ which is appropriate for narrow resonances. This cross section is easily generalized when considering not only the free proton, but also the in medium corrections to the

proton. To do this we simply replace $xg_p(x,Q^2)$ with $xG_A(x,Q^2)$ where $G_A(x,Q^2) = g_p(x,Q^2) \times R_g^A(x,Q^2)$ is the gluon distribution in the nucleus.

$F(t)$ is the nuclear form factor and is usually given by the Fourier transform of the nuclear density: $F(t) = \int \rho(r) e^{i\boldsymbol{q}\cdot\boldsymbol{r}} d^3r$ where the momentum transferred is q. The density distribution for a heavy nucleus is often modeled as a Woods-Saxon distribution,

$$\rho(r) = \frac{\rho_0}{[1 + e^{\{(r-R_A)/d\}}]},$$

where R_A is the radius of the nuclei, d is the skin depth, and ρ_0 is the central density. For our calculations we use $\rho_0 = 0.16$ /fm^3, $R_A = 1.2A^{1/3}$ fm, and $d = 0.549$ fm. There is no analytical solution to the Fourier transform of a Woods-Saxon potential. To speed up calculations, we use a convolution of a hard sphere with a Yukawa term (modified hard sphere). This gives a closed form for the nuclear form factor

$$F\left(q = \sqrt{|t|}\right) = \frac{4\pi\rho_0}{Aq^3}[\sin(qR_A) - qR_A\cos(qR_A)]\left[\frac{1}{1 + a^2q^2}\right]$$

where $a = 0.7$ fm is the Yukawa term. This formula agrees extremely well with the Fourier transform of a Woods-Saxon distribution.

Finally, we can relate the rapidity of the meson, y, to the photon energy k using the simple relationship

$$k = \left(\frac{M_V}{2}\right)e^y.$$

Using this relationship we can express the differential cross section of interaction with respect to the rapidity as

$$\frac{d\sigma^{\gamma A \to VA}}{dy} = k\frac{dN_\gamma(k)}{dk}\sigma^{\gamma A \to VA}(k).$$

Chapter 3

METHOD OF PROCEDURE

Design of Study

This work was mainly computational. The methods were derived using well established equations and models for both the nucleon degrees of freedom as well as the quark degrees of freedom.

Once the various PDF data sets were collected, they were used as the starting point for our UPC calculations. All of the PDF sets used were from highly reputable particle physics groups. The data collected pertaining to the hadronic model discussed previously was collected from within the extensive CRISP software package and was analyzed in a similar fashion to the PDF data.

Selection of Sample

The work detailed here was mostly computational. Therefore, it did not require any human participation or interaction. The models that were used to obtain the theoretical results were from highly reputable nuclear and particle physics groups. The PDFs used in this study were taken from models associated with highly cited papers. The results obtained from purely hadronic interactions were calculated in accordance with the models used by the CRISP code. Once the theoretical results were obtained, they were compared to experimental results obtained at accelerators, such as the LHC at CERN. The LHC is the world's largest and most powerful particle accelerator and is part of CERN's accelerator complex. CERN is the European Organization for Nuclear Research and currently has 21 member states. The experimental results were taken from highly cited, peer reviewed journal articles.

Collection of Data

Most of the data used in this work was self generated. However, the PDFs that were used when considering the sub-nucleonic degrees of freedom were from reputable sources. In this work I considered the MSTW09 set by Martin, Stirling, Thorne, and Watt MSTW09 (2009), the CT15 set by Dulat and collaborators (2015), the CJ12 set by Owens, Accardi and Melnitchouk (2013), and the META set by Gao and Nadolsky (2014). The minimum Q value that the PDFs were calculated at using the META framework is $Q_0 = 8$ GeV. This is above the Q values that were used in this work. As a result, the parton distribution function values for the META PDF set were found using extrapolation. These PDF sets are updates to previously published sets and include fits from additional experimental data. When considering the in medium effects, I used the EPS08 set by Eskola, Paukkunen, and Salgado (2008). These set was only available as a correction to leading order PDFs and was therefore only used in conjunction with leading order PDFs. I also used the EPS09 updates by Eskola, Paukkunen, and Salgado (2009). These sets were available as corrections to leading order and next to leading order PDFs. The HKN07 sets were developed by Hirai, Kumano, and Nagai (2004). These were only used as corrections to next to leading order PDF sets. Also used in this work were the nDS sets by de Florian and Sassot (2004). These were used as corrections to leading order and next to leading order PDFs. The final set of nuclear correction was the nCT15 distribution by Kovařík and collaborators (2015). These PDF sets contained information regarding a proton bound in lead. Therefore, they were not used as a correction on top of a free proton PDF set. The single photon cross section for the hadronic interactions was obtained from the CRISP code. In both situations above (PDF and CRISP) the equivalent photon method was implemented by using highly cited and thoroughly vetted models.

Chapter 4

PRESENTATION OF FINDINGS

Implementation of the Equivalent Photon Method

As discussed in Chapter 2, I have calculated the flux due to the nucleus of charge Z (82 for lead) to be

$$\frac{dn}{dk} = \frac{2Z^2\alpha}{\pi k}\left[\zeta K_0(\zeta)K_1(\zeta) - \frac{\zeta^2}{2}(K_1^2(\zeta) - K_0^2(\zeta))\right].$$

This flux was calculated in code that was written specifically for this work. The flux is strongly dependent on the reduced adiabacity parameter: $\zeta = 2kR/\gamma$. When using this equation it was important to distinguish which Lorentz factor is appropriate for the frame of reference being used. For this work I used γ_L which is the Lorentz factor calculated in the lab frame. Similar calculations can also be completed using the Lorentz factor that has been "boosted" to the frame of reference of one of the nuclei. The relationship between the two is

$$\gamma_{boosted} = 2\gamma_L^2 - 1 \approx 2\left(1.0735\frac{E}{A}\right)^2.$$

The equivalent photon spectrum is found by multiplying the given flux by the photon energy. This can be seen in Figure 4.1 where the equivalent photon spectrum was calculated in the frame of reference of one of the target nuclei. This was done for easier comparison to similar data in publications.

Nucleon Degrees of Freedom

The calculations using nucleonic degrees of freedom to find the differential cross section of the J/psi, which is a vector meson, do seem to match experimental data. It is noted that the experimental CMS data is slightly outside of the predictions, but only by a few percent. The results from these calculations can be seen in Figure 4.2 (E. Segundo, personal communication,

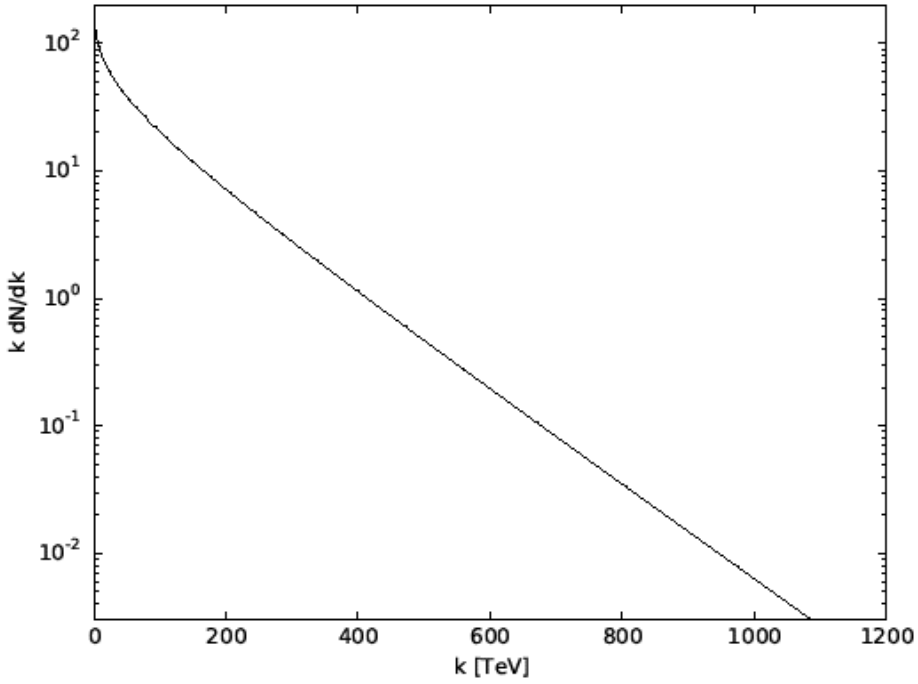

Figure 4.1: Equivalent photon spectrum evaluated in the rest frame of the target nucleus for a PbPb collision at the LHC at CERN.

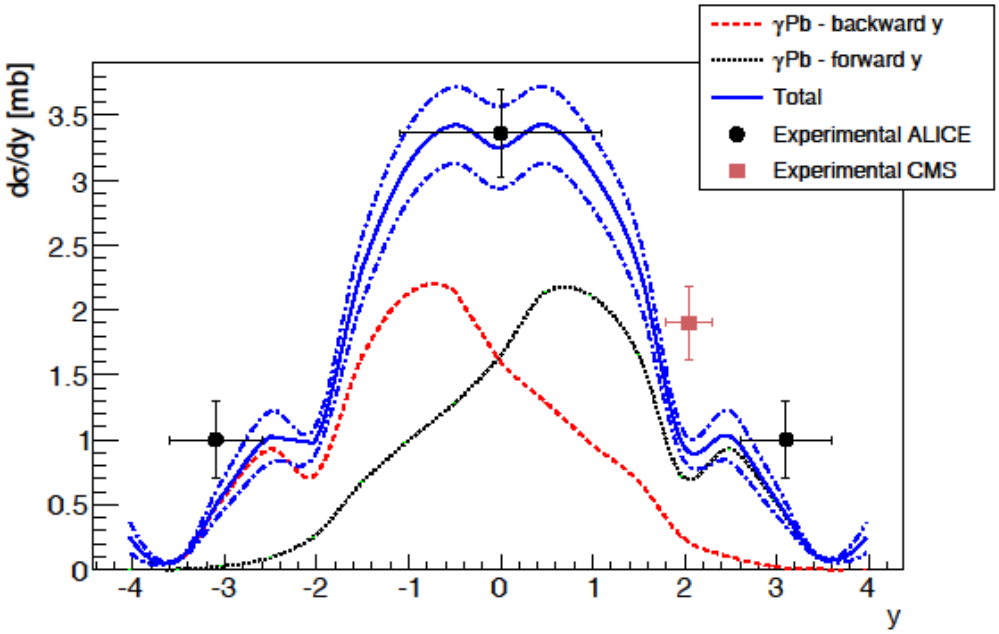

Figure 4.2: Total photoproduction of J/psi using nucleonic degrees of freedom. The dashed red line is the calculations for the forward reaction; the dotted black line shows the backward reaction. The solid blue line represents the total production (forward plus backward) and the dash-dotted blue lines represent the error bars.

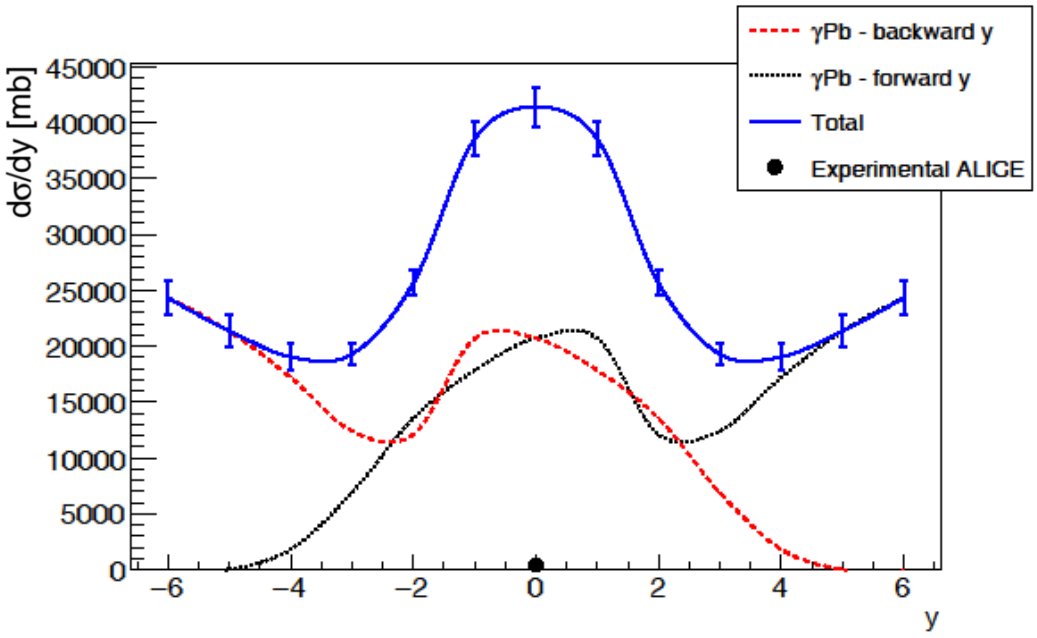

Figure 4.3: Total photoproduction of ρ^0 vector mesons. The experimental data point is at 420 mb.

March 30, 2015). The experimental ALICE data plotted is the sum of the coherent and the incoherent photoproduction and was collected by the ALICE Collaboration (Abbas et al., 2013). Experimental data from the CMS collaboration was published by the CMS collaboration (2012). Equivalent calculations were done on the ρ^0 vector meson. The results can be seen in Figure 4.3. Experimental ALICE data was collected by the ALICE Collaboration (Mayer, 2014). It is immediately seen that the models implemented by the CRISP codes significantly overestimates the production of ρ^0 vector mesons.

Quark Degrees of Freedom

When exploring the quark degrees of freedom, I present many results starting with J/psi. The J/psi particle is the second lightest charmonium particle and is the first excited state of a charm quark and anti-charm quark. It has a rest mass of 3097 MeV/c^2 and a lifetime of around 10^{-20}s. In Figure 4.4 I show the production of J\psi using the PDFs calculated for the free

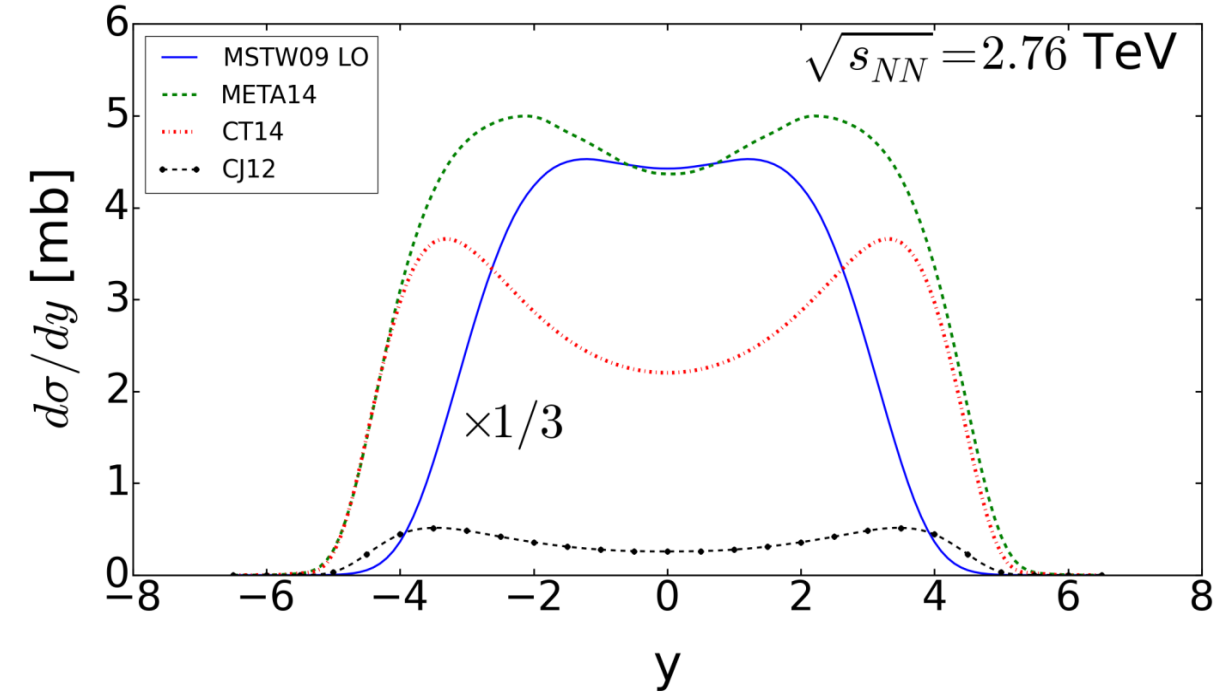

Figure 4.4: Rapidity distribution for J/Psi photoproduction calculated at $\sqrt{s_{NN}} = 2.76$ TeV. No in medium corrections are included.

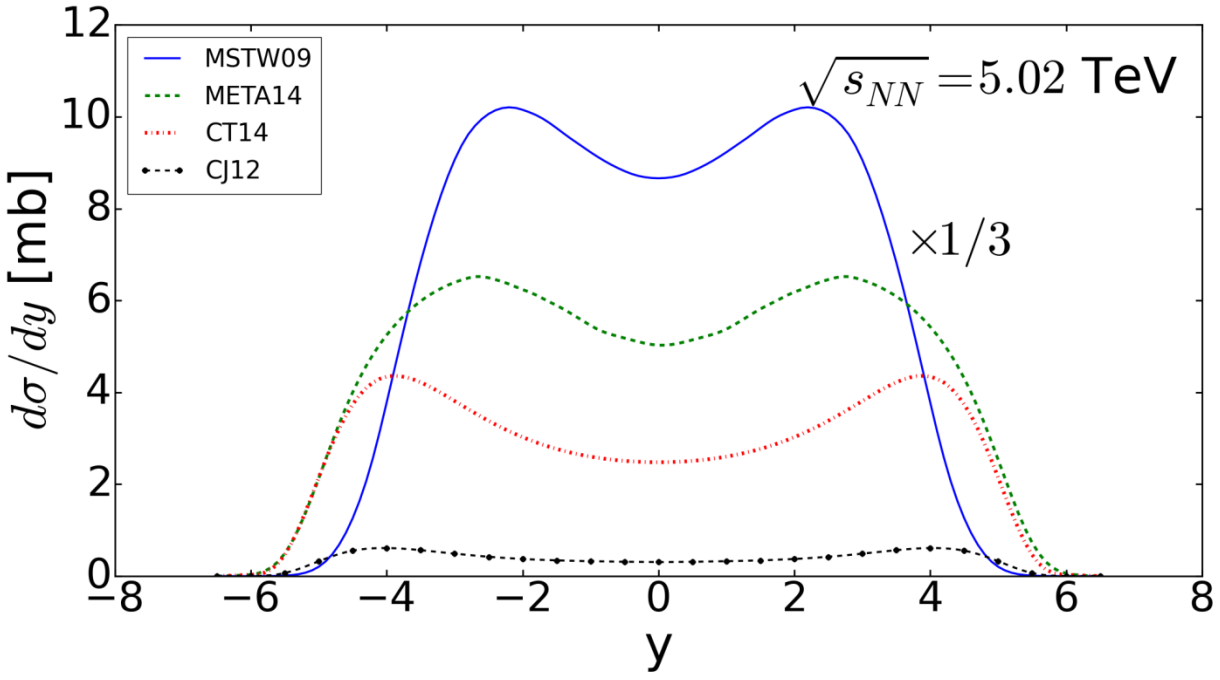

Figure 4.5: Rapidity distribution for J/psi production calculated for $\sqrt{s_{NN}} = 5.02$ TeV. No in medium corrections are considered.

protons, that is, without in medium effects. This and subsequent figures do not include the experimental data. The experimental data was included in Figure 4.17. These calculations were completed for the collision energy of $\sqrt{s_{NN}} = 2.76$ TeV which corresponds to a Lorentz factor in the lab frame of $\gamma_L = 2930$. The MSTW09 LO calculation has been multiplied by a factor of 1/3 for easier visualization. Since it is a leading order PDF, the MSTW09 calculations also included a factor of $\zeta_{J/Psi} = 1/3.5$, all of the other distribution sets are NLO and therefore did not require a correction factor for the higher order effects. It can be seen that in the case of the J/psi, the use of higher order PDF sets caused a dramatic decrease in the rapidity distributions, especially at midrapidities. The META14 and CT14 PDF sets both led to decrease in the rapidity distribution at midrapidities by a factor of about 5, while the CJ12 PDF set led to an even more significant decrease in the rapidity distribution. It should be noted that in the case of the J/psi, we use $Q = \frac{M(J/Psi)}{2} \approx 1500$ MeV which is at the bottom of Q space for the MSTW09, CT14, and CJ12 PDF sets. This value is below the lowest Q value calculated for the META14 set and the gluon distribution function was found via extrapolation in this case. Since the PDF sets all change quickly at low Q, one should expect the results to change rather dramatically if a different average momentum transfer is used.

Figure 4.5 shows the differential cross sections for the J/psi vector meson calculated at the higher nucleon-nucleon energy $\sqrt{s_{NN}} = 5.02$ TeV. This energy corresponds to a Lorentz factor in the lab frame of $\gamma_L = 5350$. Similar trends are seen in both energies. The differential cross section was significantly decreased when we used the NLO PDF sets. It is evident that the MSTW09, META14, CT14, and CJ12 all led to significantly different predictions of the rate of J/psi production.

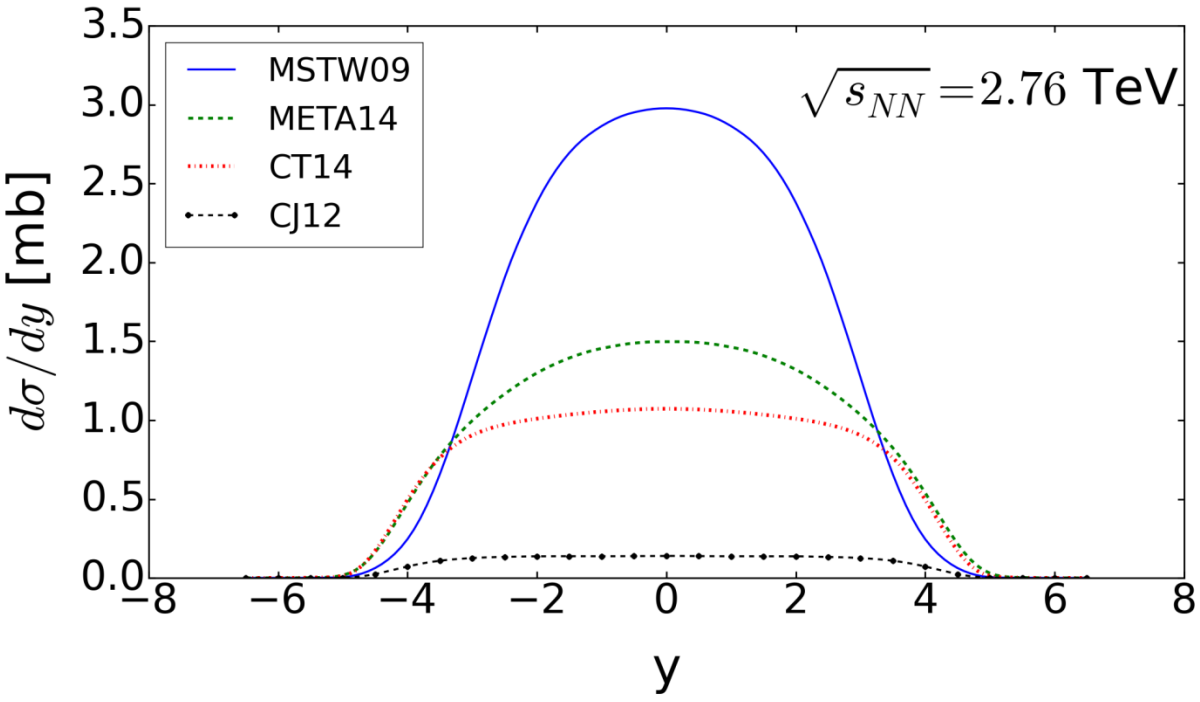

Figure 4.6: Rapidity distributions for the photo-production of the psi(2S) vector meson without nuclear medium corrections.

Next, we considered the photoproduction of the psi(2S) meson. This meson is the first excited state of the J/psi and is also a member of the charmonia family. It has a rest mass of 3686 MeV/c^2 and a mean lifetime on the order of 10^{-20}s. Figures 4.6 and 4.7 show the rapidity distributions for the photoproduction the psi(2S) at $\sqrt{s_{NN}} = 2.76$ TeV and $\sqrt{s_{NN}} = 5.02$ TeV. In Figure 4.6 it can be seen that the MSTW09 LO calculations still led to the largest cross sections, however they now were only larger by a factor of about 2 instead of a factor of 4 as they were for the J/psi. It can also be seen that the multiple humps present in the J/psi rapidity distributions were no longer present. The difference in shapes of the distribution was a result of differences in the PDF. The difference in the magnitude was due to the mass dependence of the forward scattering amplitude on the vector meson mass: $\sigma^{\gamma A \to VA} \propto 1/M_V^5$. This meant that a relatively small change in the mass, such as going from the J\psi to the psi(2S), would cause a large

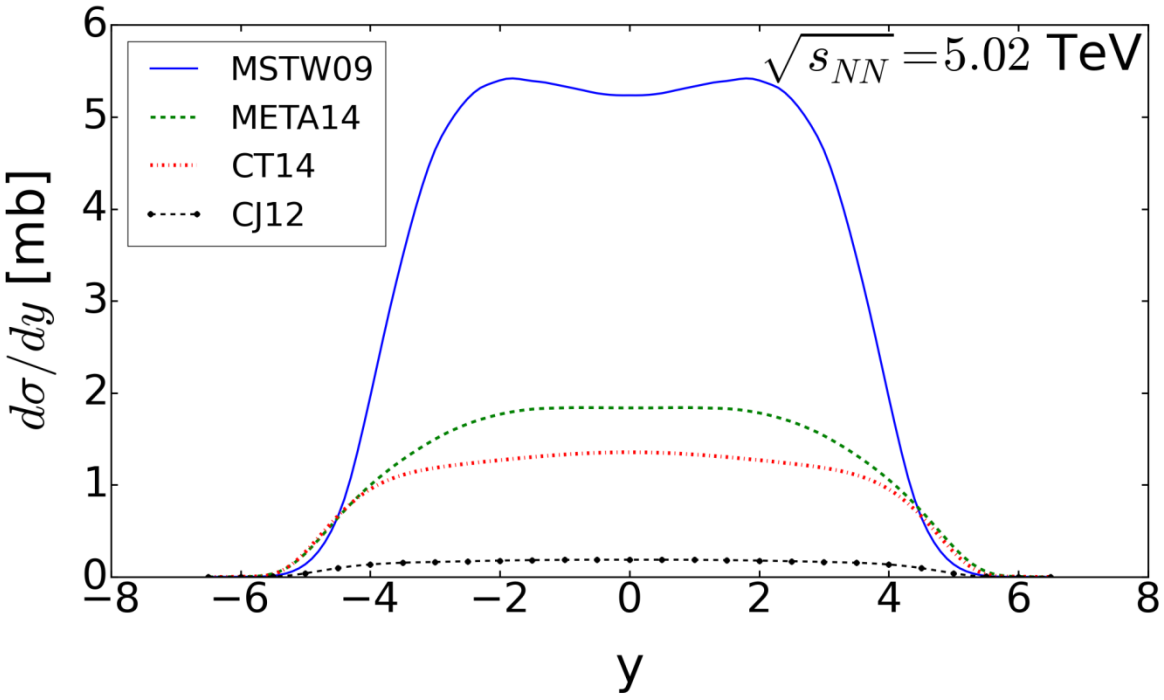

Figure 4.7: Rapidity distribution for the production of psi(2S) vector mesons without including corrections for in nucleus effects.

difference in the differential cross section. Similar trends were also seen at the higher collision energy. The MSTW09 rapidity distribution was larger than the META14 and CT14 distributions by a factor of about 3, and the CJ12 distribution was much smaller than the others. It was also seen that the "double hump" has returned to the MSTW09 distribution. This was because the higher collision energy allowed for more high energy photons. These photons, in turn, allowed more production at larger and larger absolute rapidities.

The final vector meson that was considered in this work was the Upsilon. It has a rest mass of 9460 MeV/c^2 and a lifetime similar to the J/psi. Unlike the J/psi and the psi(2S), the Upsilon consists of a bottom quark and an anti-bottom quark. Figure 4.8 shows the rapidity distributions for the production of the Upsilon vector meson at the lower energy of $\sqrt{s_{NN}} = 2.76$ TeV. The results presented in this figure are in units of μb instead of the mb that the results for

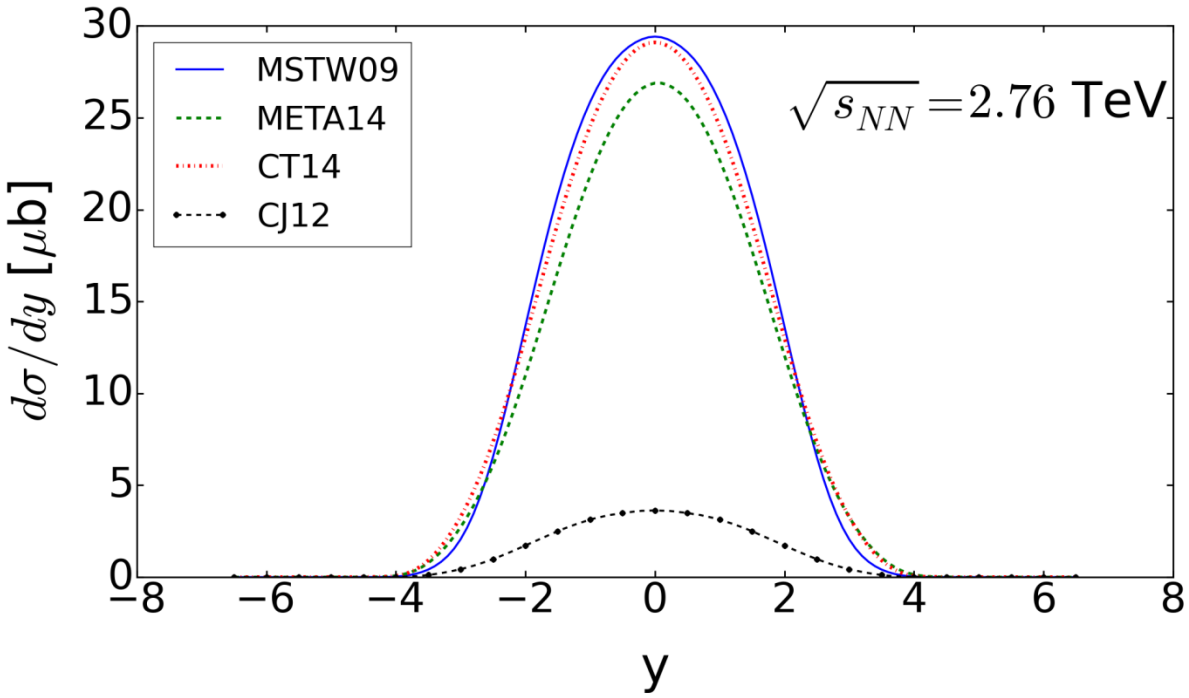

Figure 4.8: Rapidity distributions for the production of the Upsilon vector meson without the inclusion of in medium corrections.

the J\psi and the psi(2S) were presented in. This decrease in the production by three orders of magnitude was due to a combination of two factors. Since the forward scattering amplitude is inversely proportional to the mass raised to the fifth power, the increased mass of the Upsilon caused a significant change in the rapidity distributions. The decrease was also a result of there being fewer quasi-real photons in this energy region. It was also seen that the MSTW09, META14, and CT14 rapidity distributions were all very similar to each other. This meant that the contribution from higher order effects in the PDFs were much smaller at this Q scale than they were for the Q values considered for the lighter mesons. This smallness of higher order effects was in agreement with what was found by Adeluyi and Bertulani in their work (2011). The rapidity distribution from the CJ12 PDF was still significantly smaller than the others shown. Figure 4.9 shows the rapidity distributions for the production of the Upsilon meson at the higher collision energy. It can be seen that the distributions increased by a factor of about 2 at the

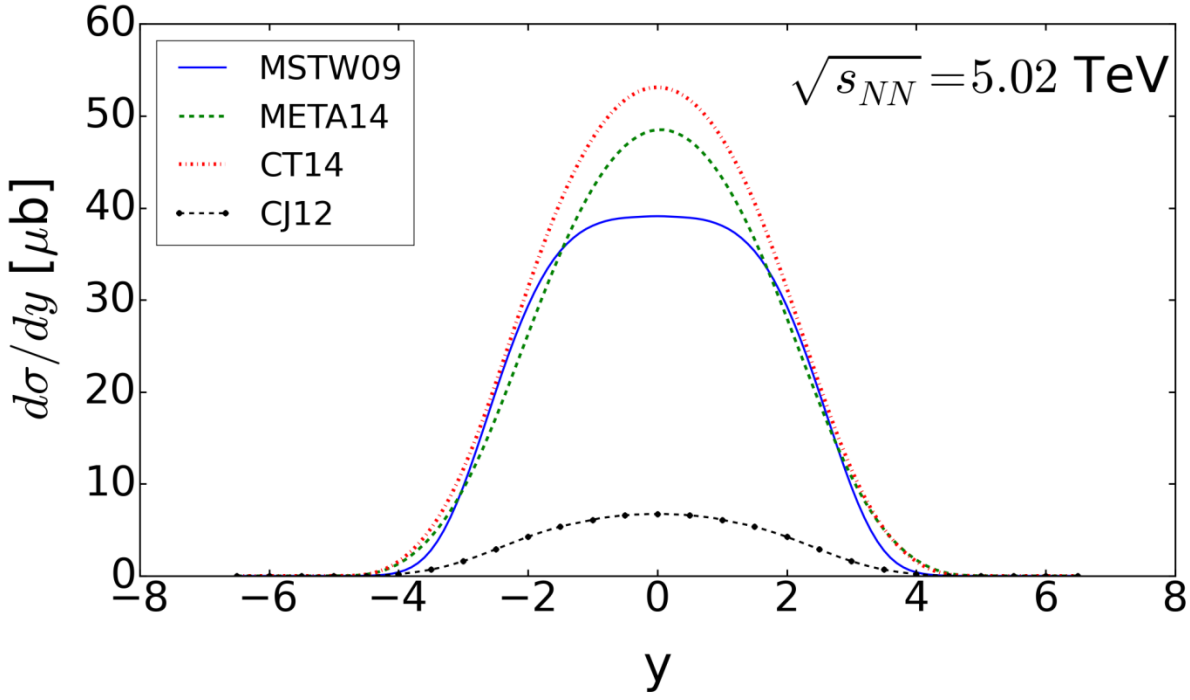

Figure 4.9: Rapidity distributions for the production of the Upsilon vector meson without the corrections for in medium nuclear effects.

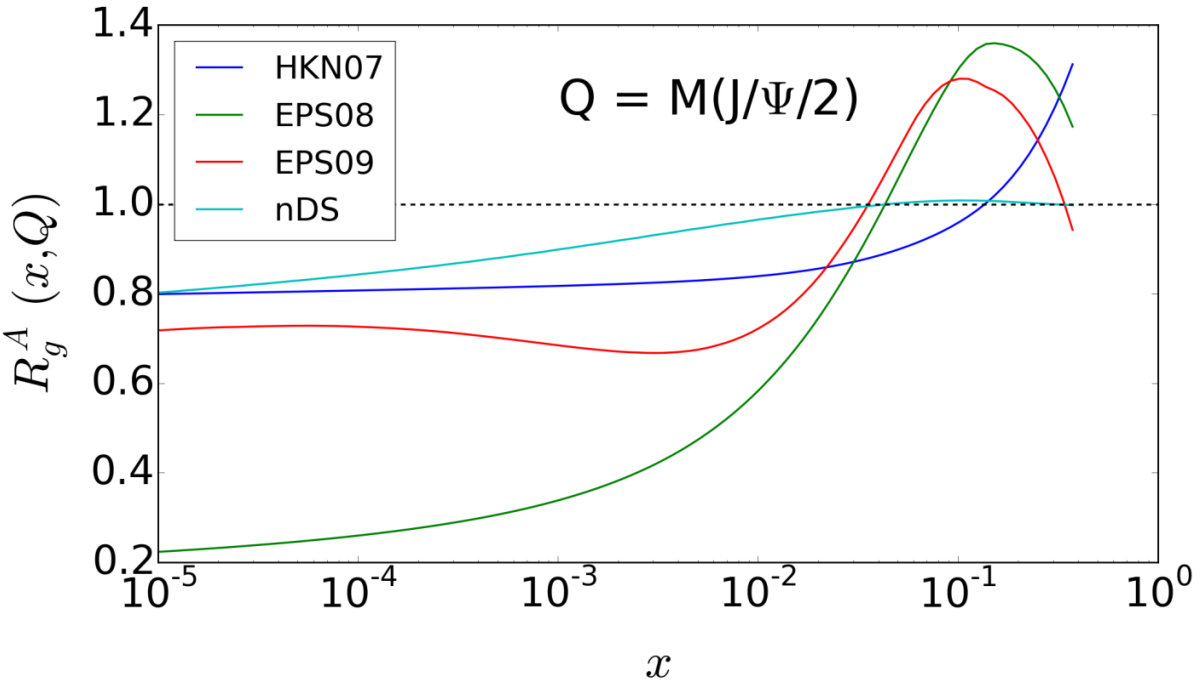

Figure 4.10: Sample nuclear correction factors for a proton bound in lead 208. The dotted line at 1.0 is present for easier viewing of the shadowing and antishadowing regions.

higher energy and that the MSTW09 rapidity distribution exhibited some suppression at midrapidities. The CJ12 rapidity distribution remained much smaller than the others considered.

Quark Degrees of Freedom with in Medium Effects

Next I considered how in medium corrections modified the rapidity distributions. The nuclear modifications are generally categorized by different domains of x. At small values of x the nuclear modification is generally less than unity and therefore the nuclear parton distribution function is less than the corresponding distribution function for free protons. Because of this depletion, the region of $x \lesssim 0.04$ is said to exhibit the phenomenon generally called shadowing. An increase of the nuclear parton distribution function compared to the PDF of the free proton occurs in the domain $0.04 \lesssim x \lesssim 0.3$. This phenomenon is usually called antishadowing. Another decrease is generally present over the domain $0.3 \lesssim x \lesssim 0.8$. For $x \gtrsim 0.8$ an enhancement is present due to the Fermi motion of the partons. These effects can be seen in Figure 4.10. The figure also shows the relative strengths of the shadowing and antishadowing effects. The HKN07 correction factors did not show any antishadowing except what is due to the Fermi motion. The nDS distribution showed the shadowing and antishadowing phenomena, but only very weakly. The EPS08 and EPS09 correction factors both showed the shadowing and antishadowing effects with EPS08 exhibiting the strongest effects of the nuclear correction factors considered in this work.

Figure 4.11 shows the rapidity distributions calculated when we take into account the nuclear correction factors. In the upper pane of the figure I show the CT14 free proton rapidity distribution along with the rapidity distribution when we also used nuclear correction factors. The lower pane shows similar calculations, but using META14 as the free proton PDF. Also shown on both the upper and lower pane is the nCT15 rapidity distribution. Since this

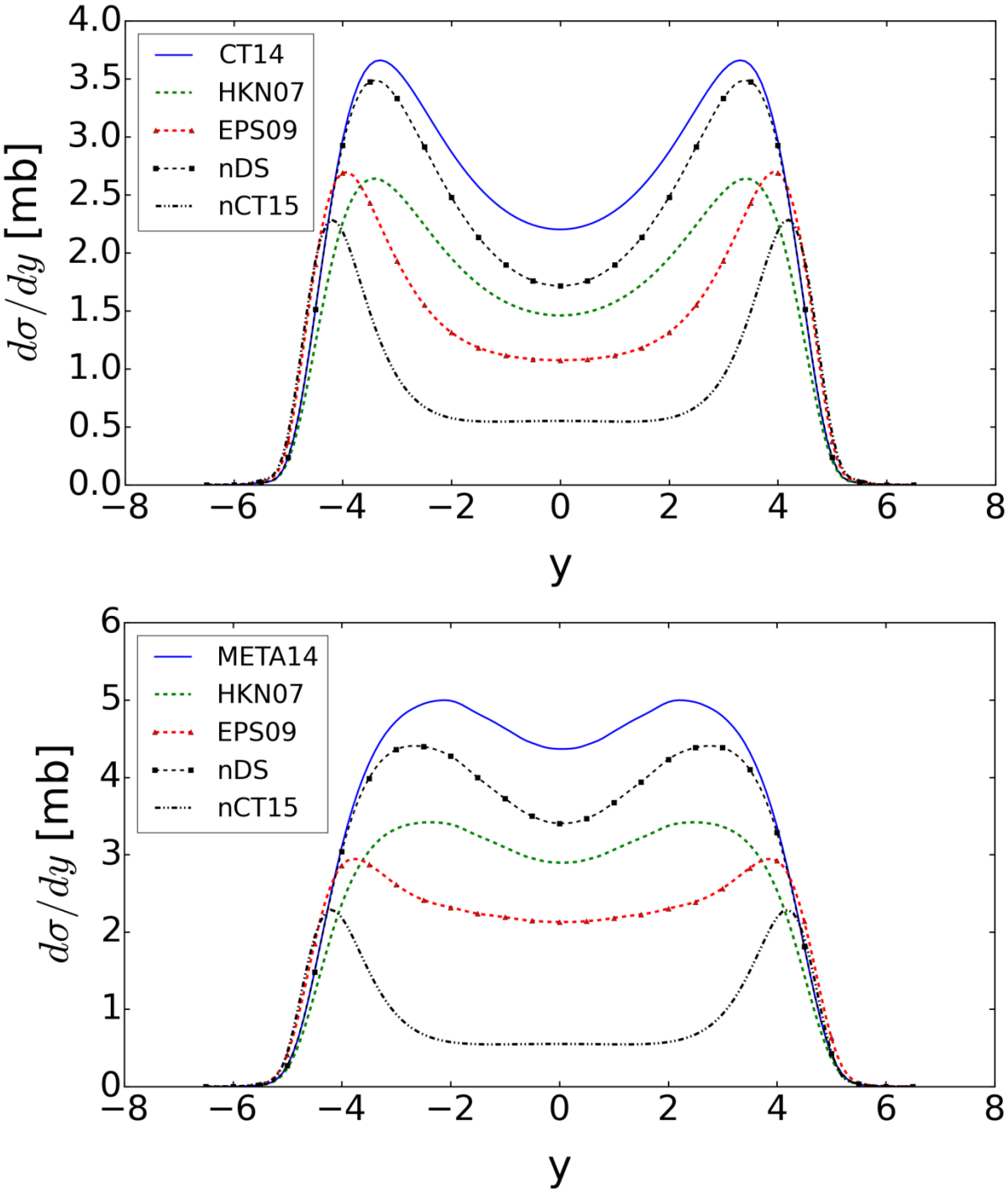

Figure 4.11: Rapidity distributions for the production of J/Psi vector mesons including nuclear corrections for $\sqrt{s_{NN}} = 2.76$ TeV. The upper figure is the CT14 free proton PDF with the HKN07, EPS09, and nDS nuclear corrections. The bottom figure is the META14 free proton PDFs with the same nuclear corrections. Also included in both cases is the rapidity distribution for the nCT15 bound proton parton distribution function.

distribution function pertained to the bound proton, the nCT15 was not a correction applied to CT14 or META14. It was shown as a comparison. In both cases it was seen that the inclusion of the nuclear correction factors decreased the overall rapidity distribution. This means that in these calculations the most relevant phenomenon exhibited by the nuclear correction factors was shadowing.

Figure 4.12 shows the rapidity distributions for the production of J/psi at the LHC with $\sqrt{s_{NN}} = 5.02$ TeV using EPS09, HKN07, and the nDS nuclear correction factors. The distribution for nCT15 was also shown for comparison. It can be seen from Figures 4.11 and 4.12 that the EPS09 led to smaller differential cross sections at midrapidity than the HKN07 or the nDS nuclear correction factors. This was because the EPS09 correction factors exhibited stronger shadowing. The HKN07 and nDS nuclear correction factors contained very little shadowing, and therefore ded not decrease the rapidity distributions as strongly. When comparing the lower energy collision $\sqrt{s_{NN}} = 2.76$ TeV to the higher energy $\sqrt{s_{NN}} = 5.02$ TeV it can be see that there was an overall increase in the differential cross section as well as a wider distribution. This was because; at the higher energy collisions there were harder photons present in the equivalent photon spectrum which allowed for more production of the vector meson.

I continued this work by considering the nuclear corrections on the psi(2S) vector meson. As discussed previously, the psi(2S) is an excited state of the J/psi with a mass roughly 20% larger than the J/psi. This increased mass caused an overall decrease in the production of the psi(2S) when compared to the J/psi. Figure 4.13 shows the rapidity distributions for the photoproduction of the psi(2s) at the LHC with $\sqrt{s_{NN}} = 2.76$ TeV when using nuclear correction factors. Inclusion of the nuclear correction factors led to similar trends for the psi(2S) meson as they did for the J/psi. The EPS09 correction factors led to a strong reduction in the production

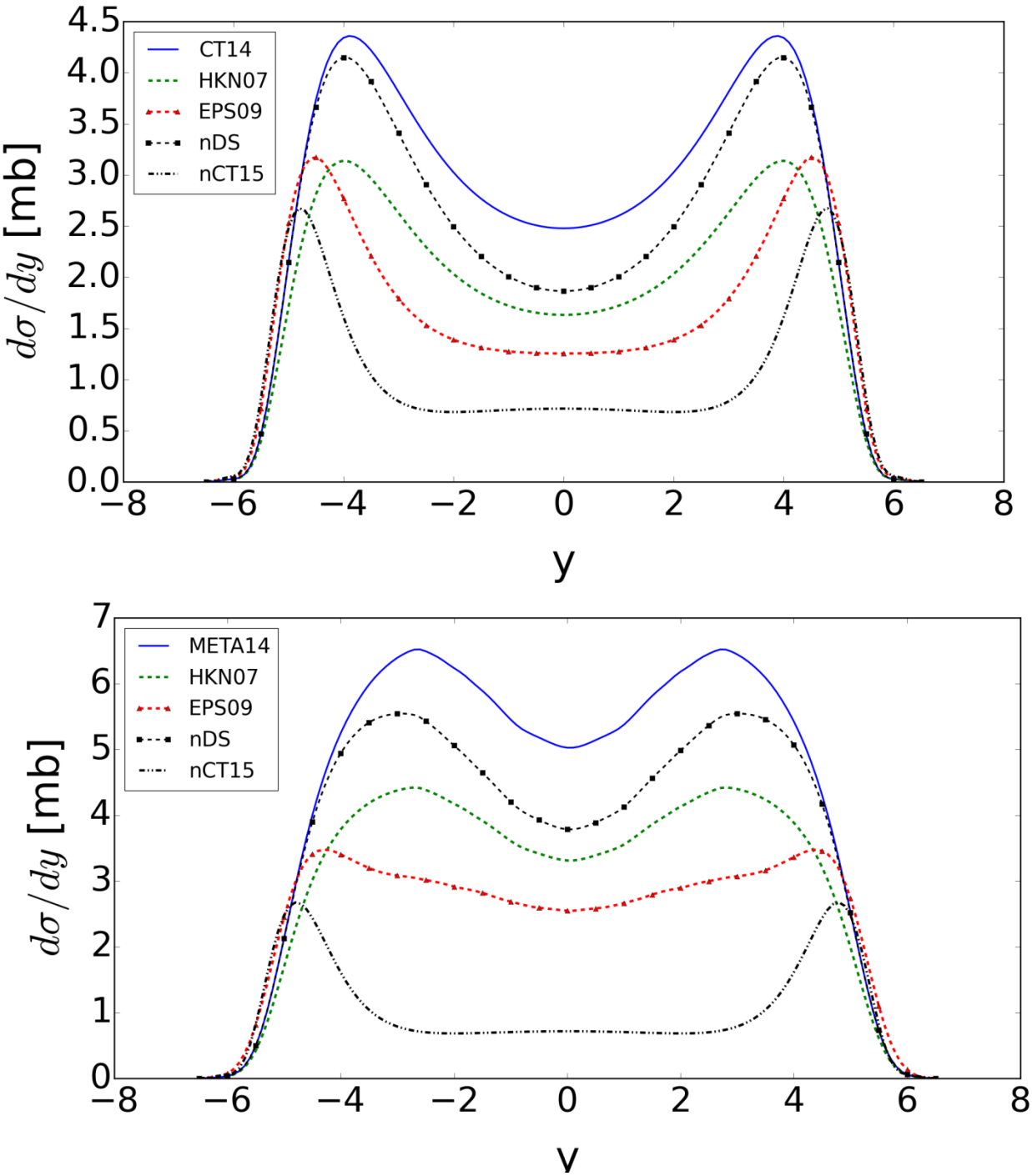

Figure 4.12: Rapidity distributions for the production of J/psi vector mesons including nuclear corrections for $\sqrt{s_{NN}} = 5.02$ TeV. The upper figure is the CT14 free proton PDF with the HKN07, EPS09, and nDS nuclear corrections. The bottom figure is the META14 free proton PDFs with the same nuclear corrections. Also included in both cases is the rapidity distribution for the nCT15 bound proton parton distribution function.

due to its strong shadowing while the nDS and HKN07 led to smaller reductions since they had little or no shadowing present. It was also noted that the nCT15 bound proton distributions were much closer to the other rapidity distributions for the psi(2S) particle. The differences in shapes of the rapidity distributions between the psi(2S) distributions and those for the J/psi were due to the sensitivity of the parton distribution functions to the Q value for low Q.

Figure 4.14 shows the rapidity distributions for the production of the psi(2S) vector meson at the LCH with $\sqrt{s_{NN}} = 5.02$ TeV. Similar trends can be seen in this Figure 4.14 as the trends previously seen when considering the photoproduction of vector mesons with nuclear correction factors.

The final particle considered here is the Upsilon. The larger mass of the vector meson had a dramatic impact on the magnitude of the cross section. The differential cross section decreased by about three orders of magnitude compared to the cross section of the previous two particles. The Upsilon also had a significantly narrower rapidity distribution for photoproduction. This was because the larger mass led to a change in the x values probed which in turn changed the forward scattering amplitude through its quadratic dependence on $xg_A(x, Q^2)$. Figures 4.15 and 4.16 show the rapidity distributions for the photoproduction of Upsilon mesons at $\sqrt{s_{NN}} = 2.76$ TeV and $\sqrt{s_{NN}} = 5.02$ TeV respectively. As with the previous particles considered, inclusion of the nuclear correction factors led to a decrease in the differential cross section, especially at mid rapidities. In the case of the Upsilon, the rapidity distribution fell off at an absolute rapidity of about 2. The previous particles' rapidity distributions had significant contributions to absolute rapidities of about 4. This decrease in the width was due to the larger mass of the Upsilon changing the momentum fraction probed.

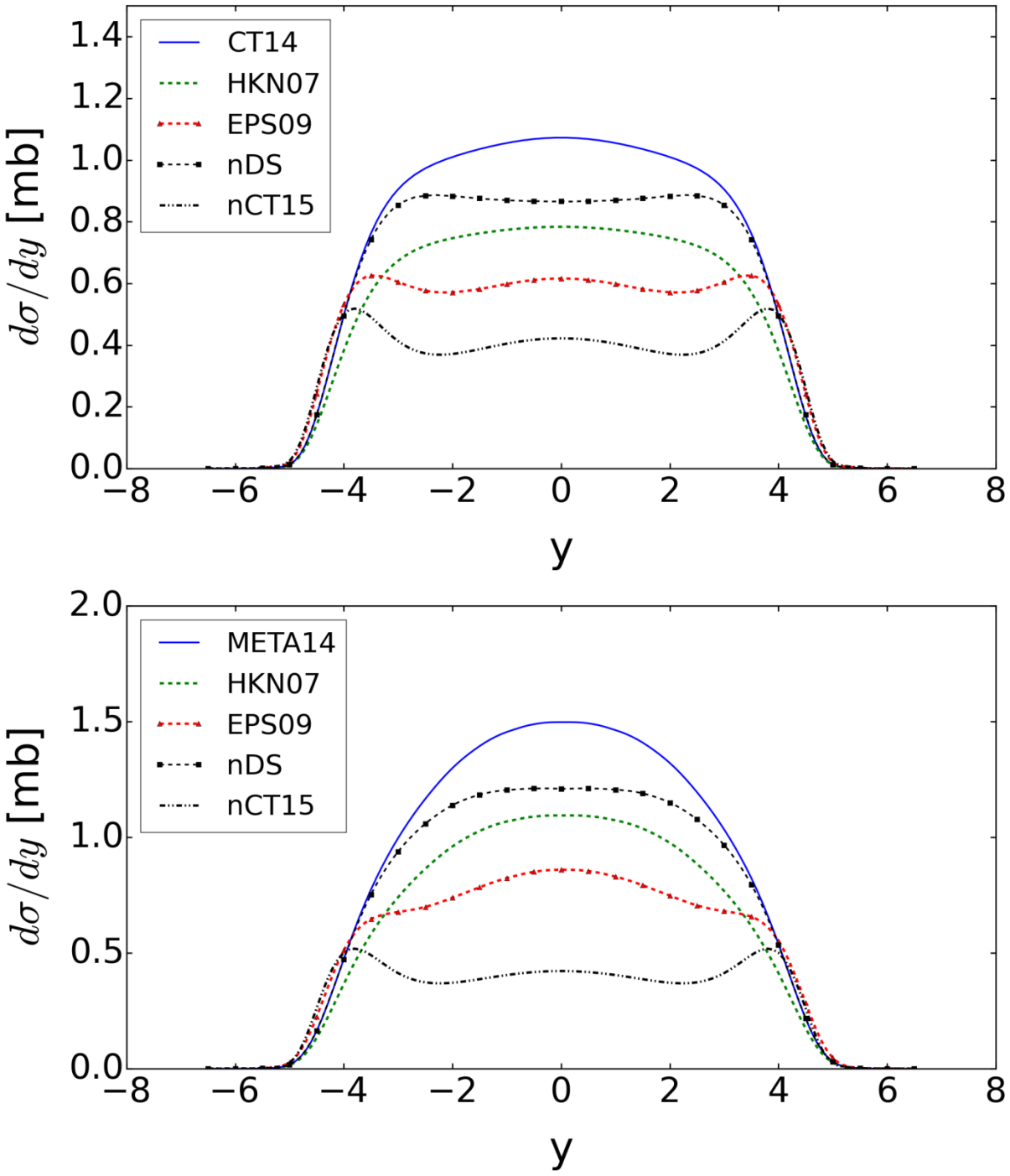

Figure 4.13: Rapidity distributions for the production of psi(2S) vector mesons including nuclear corrections for $\sqrt{s_{NN}} = 2.76$ TeV. The upper figure is the CT14 free proton PDF with the HKN07, EPS09, and nDS nuclear corrections. The bottom figure is the META14 free proton PDFs with the same nuclear corrections. Also included in both cases is the rapidity distribution for the nCT15 bound proton parton distribution function.

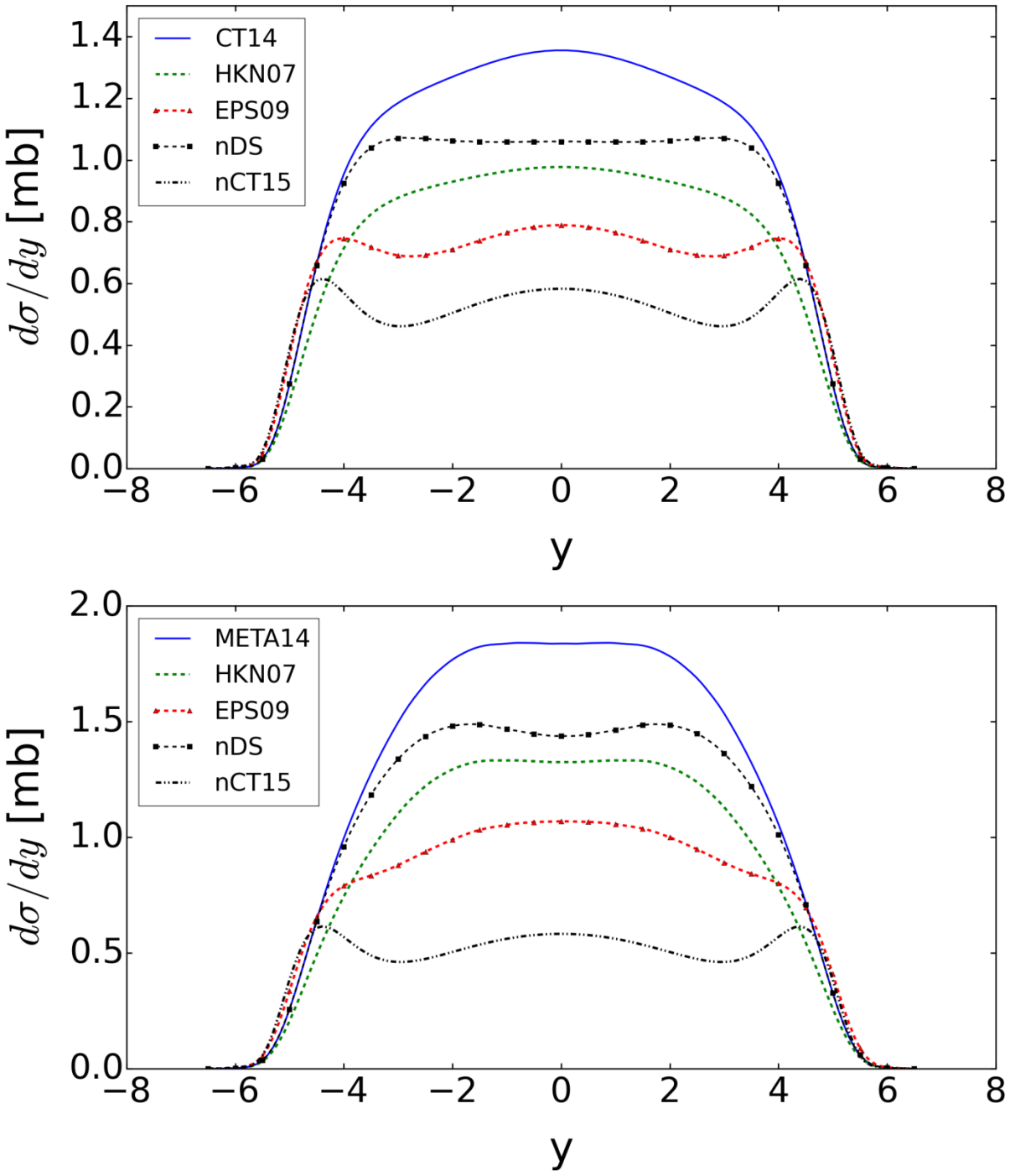

Figure 4.14: Rapidity distributions for the production of psi(2S) vector mesons including nuclear corrections for $\sqrt{s_{NN}} = 5.02$ TeV. The upper figure is the CT14 free proton PDF with the HKN07, EPS09, and nDS nuclear corrections. The bottom figure is the META14 free proton PDFs with the same nuclear corrections. Also included in both cases is the rapidity distribution for the nCT15 bound proton parton distribution function.

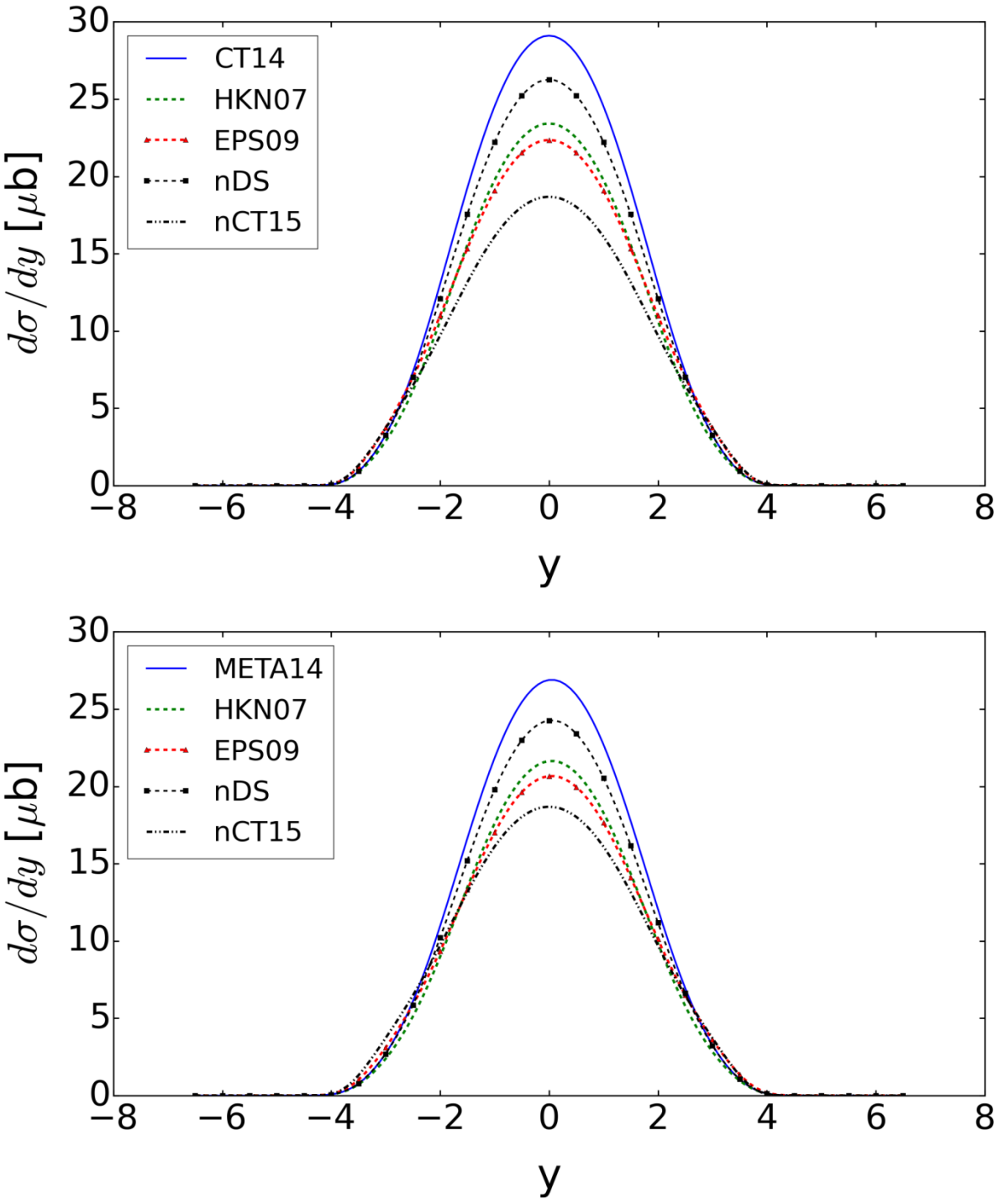

Figure 4.15: Rapidity distributions for the production of Upsilon vector mesons including nuclear corrections for $\sqrt{s_{NN}} = 2.76$ TeV. The upper figure is the CT14 free proton PDF with the HKN07, EPS09, and nDS nuclear corrections. The bottom figure is the META14 free proton PDFs with the same nuclear corrections. Also included in both cases is the rapidity distribution for the nCT15 bound proton parton distribution function.

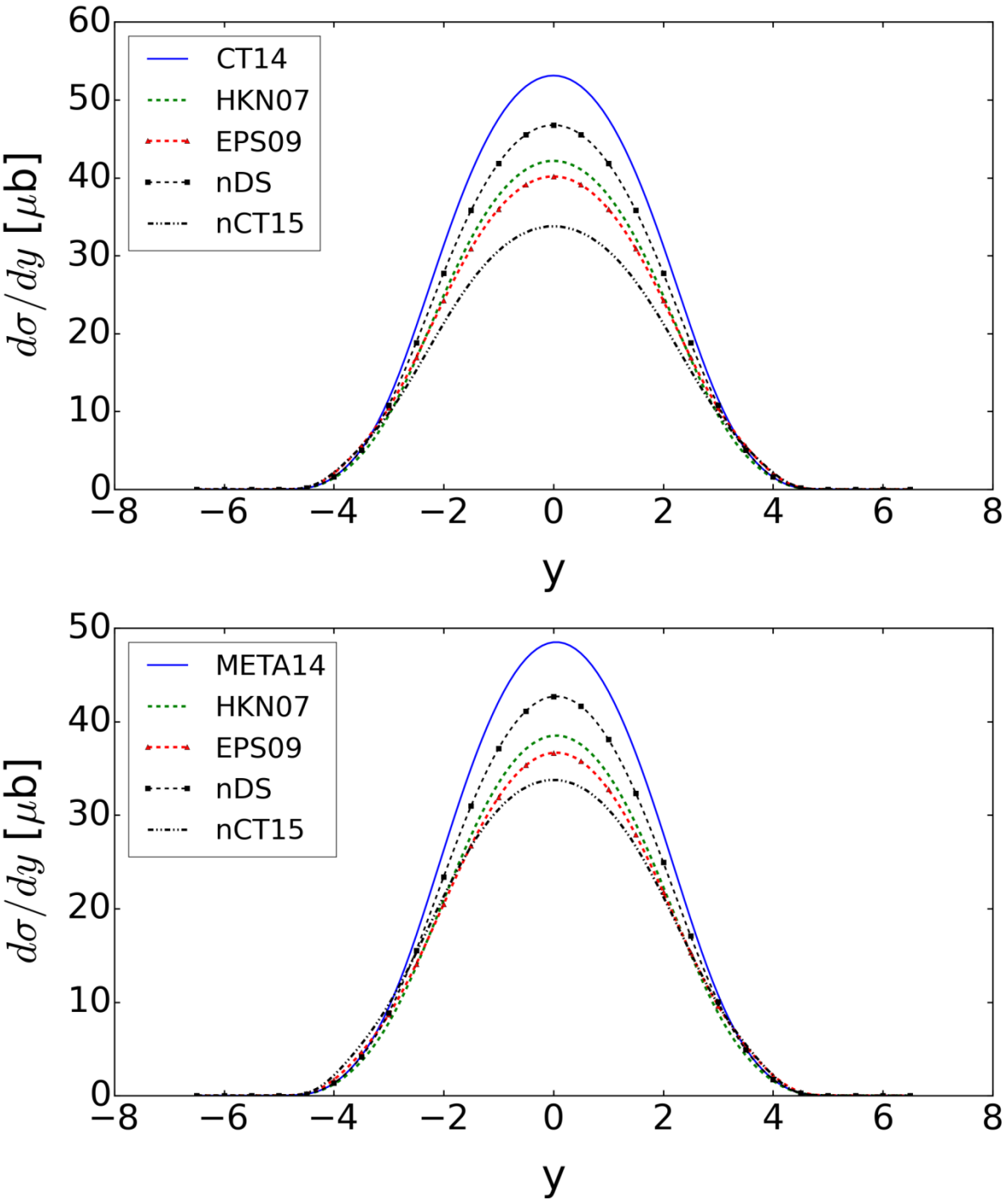

Figure 4.16: Rapidity distributions for the production of Upsilon vector mesons including nuclear corrections for $\sqrt{s_{NN}} = 5.02$ TeV. The upper figure is the CT14 free proton PDF with the HKN07, EPS09, and nDS nuclear corrections. The bottom figure is the META14 free proton PDFs with the same nuclear corrections. Also included in both cases is the rapidity distribution for the nCT15 bound proton parton distribution function.

PDF	2.76 TeV	5.02 TeV
MSTW 09 LO	83	220
+ EPS 08	7.8	16
+ EPS 09	42	113
+ nDS	62	155
META 14	11	16
+ HKN 07	8.0	11
+ EPS 09	6.6	9.1
+ nDS	10	14
CT 14	7.5	10
+ HKN 07	5.3	6.9
+ EPS 09	4.6	5.9
+ nDS	6.7	8.6
CJ12	1.0	1.3
+ HKN 07	0.7	0.9
+ EPS 09	0.6	0.8
+ nDS	0.9	1.1
nCT15	2.9	3.4

Table 4.1: Cross sections (in mb) for J/psi production in UPCs at the LCH for two laboratory energies and several parton distributions and nuclear correction factors

Total Cross Sections

In addition to the differential cross sections presented above, I also studied the total cross sections for the photoproduction of the vector mesons. These were calculated for the MSTW09 (leading order), META14 (next to leading order), CT14 (next to leading order), and CJ12 (next to leading order) free proton PDF sets. Also included were the total cross sections for the free proton PDF sets mentioned above with nuclear correction factors. The EPS08, EPS09, and nDS nuclear correction factors were used with the leading order PDF sets since they were available as leading order corrections. The HKN07, EPS09, and nDS nuclear correction factors were used with the next to leading order PDF sets. The nCT15 total cross section was included as well. Since the PDF sets used in the case of nCT15 were for the proton bound in lead 208, they are stand alone calculations and were not multiplied by a free proton PDF. Table 4.1 shows the total cross sections for the production of J/psi vector mesons. As was seen in the differential

PDF	2.76 TeV	5.02 TeV
MSTW09	1.6	3.8
+ EPS08	0.33	0.64
+ EPS09	0.72	1.6
+ nDS	1.4	3.2
META14	10	14.7
+ HKN07	7.5	10.8
+ EPS09	6.5	9.3
+ nDS	8.9	12.6
CT14	8.0	11.3
+ HKN07	6.0	8.4
+ EPS09	5.3	7.3
+ nDS	7.1	9.8
CJ12	1.1	1.6
+ HKN07	0.81	1.2
+ EPS09	0.72	1.0
+ nDS	1.0	1.4
nCT15	3.9	5.5

Table 4.2: Total cross sections (in mb) for psi(2S) production in UPCs at the LHC for two laboratory energies and several parton distributions and nuclear correction factors.

cross sections, the MSTW09 parton distribution functions led to the largest cross sections at both energies. The META14 and CT14 total cross sections were all smaller than the MSTW09 cross sections by a factor of about 3. This indicated that there were significant processes occurring at higher orders in the production of the J/psi. The nCT15 total cross sections were about the same as the CT14 with the EPS08 nuclear correction factors. Since the CT14 free proton PDF sets and the nCT15 bound proton PDF sets both came from the CTEQ collaboration I expected this similarity.

Table 4.2 shows similar data that was calculated for the psi(2s) vector meson. The MSTW09 cross sections were still the largest, but now they are only larger than the cross sections for the META14 and CT14 PDFs by a factor of 2. This showed that the higher order processes are still present, but did not contribute as significantly to the suppression of the

PDF	2.76 TeV	5.02 TeV
MSTW09	11	31
+ EPS08	5.7	14
+ EPS09	7.5	20
+ nDS	10	28
META14	101	211
+ HKN07	82	168
+ EPS09	82	166
+ nDS	92	188
CT14	111	237
+ HKN07	90	189
+ EPS09	90	186
+ nDS	101	211
CJ12	14	31
+ HKN07	12	25
+ EPS09	11	16
+ nDS	13	24
nCT15	78	161

Table 4.3: Cross sections (in μb) for Upsilon production in UPCs at the LHC for two laboratory energies and several parton distributions and nuclear correction factors.

production of the psi(2s) as they did for the production of J/psi. The nCT15 total cross section was comparable to the CT14 free proton PDF with the EPS09 correction factors.

Table 4.3 shows the total cross sections for the Upsilon vector meson. In this case, the predictions made using the MSTW09 PDF set were comparable to those made using the META14 and the CT14 at the lower energy of $\sqrt{s_{NN}} = 2.76$ TeV. At the higher energy, the total cross section predicted using the MSTW09 PDF set was slightly smaller than the cross section calculated using the next to leading order PDF sets. This indicated that the higher order processes are small at this energy scale. The nCT15 total cross section was very similar to the cross sections calculated using the CT14 free proton PDF set along with the EPS09 nuclear correction factors.

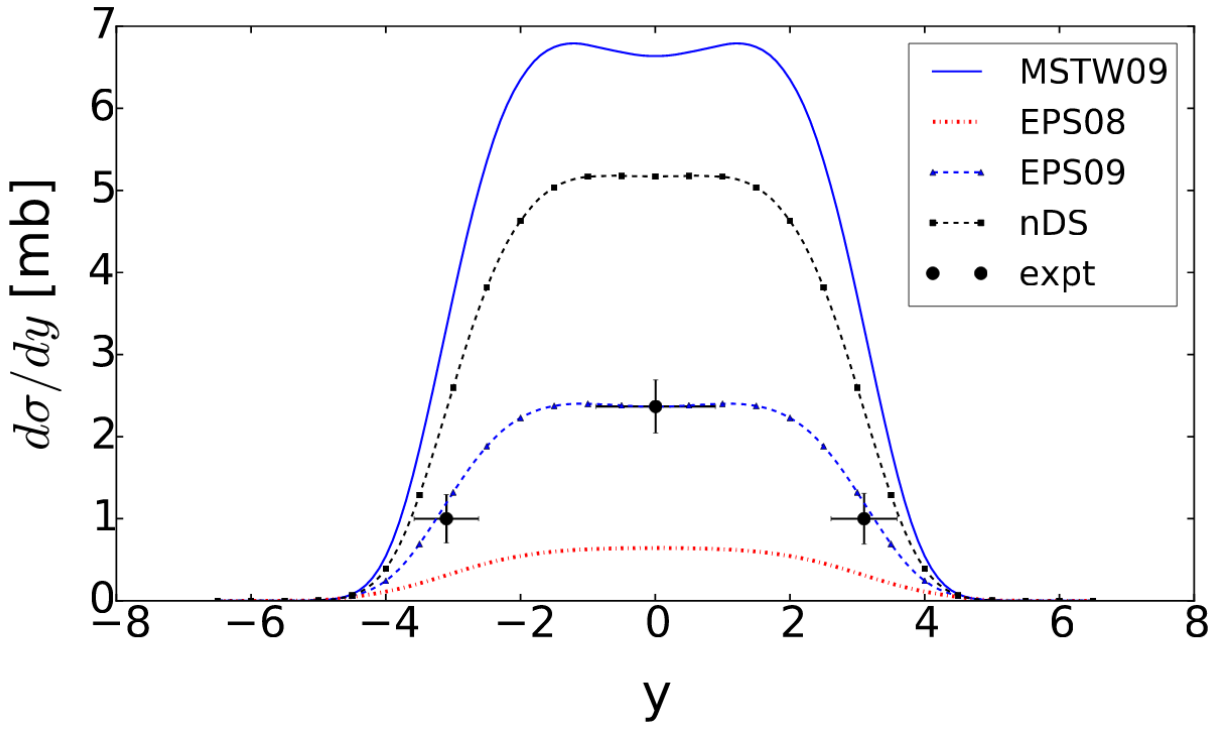

Figure 4.17: Coherent production of the J/psi vector meson using the MSTW09 leading order PDF and various nuclear correction factors.

Separation of Coherent and Incoherent Production

The ALICE collaboration defined coherent and incoherent production for production of the J/psi production (Abbas, 2013). If the transverse momentum is $P_T < 200$ MeV/c in the J/psi$\longrightarrow\mu^+\mu^-$ decay channel or $P_T < 300$ MeV/c in the J/psi$\longrightarrow e^+e^-$ channel then the collision is said to be coherent. In this case, the photon acts coherently on the whole nucleus. In this regime, the average transverse momentum is on the order of $\langle P_T \rangle \simeq 60$ MeV/c. At these transverse momenta, the interaction with the photon usually does not lead to nuclear break up as the vector meson is produced. Conversely, if the transverse momentum is $P_T > 200$ MeV/c in the J/psi$\longrightarrow\mu^+\mu^-$ decay channel or $P_T > 300$ MeV/c in the J/psi$\longrightarrow e^+e^-$ decay channel then the collision is said to be incoherent. In this regime, the photon interacts with a single nucleon instead of the whole nucleus. I only considered the coherent production of J/psi using the

MSTW09 free nucleon PDF in this work. In this situation, the distributions were reduced by a factor of about 0.5. These rapidity distributions can be seen in Figure 4.17. The ALICE collaboration found a combined weighted average for the di-electron and di-muon channels of $d\sigma^{coherent}/dy = 2.38^{+0.34}_{-0.24}$ mb at midrapidity. Our calculations for the MSTW09 and the EPS09 nuclear correction factors yielded 2.42 mb which agreed well with the experimental data. Since there was very little experimental data for the other vector mesons studied in this work, I did not consider the separation of the coherent and incoherent production for the other particles or other PDF sets.

Chapter 5

CONCLUSIONS

Summary

In the first part of this work, I studied the production of the ρ^0 and J/psi vector mesons using nucleonic degrees of freedom. In the second part of this work, the elastic photoproducion of the J/psi, psi(2S), and Upsilon vector mesons were studied in ultra-peripheral collisions at the LHC at CERN. I examined two energies: $\sqrt{s_{NN}} = 2.76$ TeV and $\sqrt{s_{NN}} = 5.02$ TeV, and focused on Pb^{208}+Pb^{208} collisions. I only considered direct photoproduction of the vector mesons. I used the MSTW09, META14, CT14, and the CJ12 free proton parton distribution functions and used the EPS08, EPS09, HKN07, and nDS nuclear correction factors. I also used the nCT15 parton distribution function for a proton bound in lead 208.

Findings

I have shown that the models based off of nucleonic degrees of freedom yielded reasonable results for the production of the J/psi vector meson. However, these models overestimated the production of the ρ^0 vector meson by two orders of magnitude. I have also shown that the rapidity distributions as well as the total cross sections derived from sub-nucleonic degrees of freedom were highly sensitive to the parton distribution function used. This was to be expected since the forward scattering amplitude is dependent on $[x g_A(x, Q^2)]^2$ (see Equation on page 19). The cross section showed a relatively weak sensitivity to antishadowing at very forward and backward rapidities and an appreciable sensitivity to shadowing at midrapidities.

Due to the small differences in mass, there were only minor differences in the shapes of the rapidity distributions for the production of the J/psi and the psi(2S) mesons. However, the

magnitude of the cross sections for the production of the Upsilon decreased by a factor of 3 because of the reduced number of virtual photons for the higher meson mass as well as the $1/M_V^5$ dependence of the forward scattering amplitude. Significant differences were seen in the shape of the rapidity distribution as well as the magnitude of the cross section when I studied the Upsilon vector meson. The magnitude of the cross section decreased by almost 3 orders of magnitude and the rapidity distribution was much narrower. I also showed that the separation of coherent and incoherent production of vector mesons can lead to distributions that can be directly compared to experimental data. When this separation was properly considered, the models using quark degrees of freedom matched the experimental data quite well.

Recommendations for Future Research

This research could be expanded upon in many areas in the future. For the nucleonic degrees of freedom, it is necessary to understand the overproduction of the ρ^0 vector meson. To decrease the cross section of the meson, it is necessary to add more final state interaction. It would also be useful to study what happens when the coherent and incoherent photoproduction are separated.

There are also many areas that the research involving the quark and gluon degrees of freedom can be expanded on. One of the most pressing areas is the proper treatment of errors associated with the rapidity distributions as well as the total cross sections. There are two main methods that could be used to estimate these errors. The Hessian method is based on the linear propagation of errors through a covariance error matrix. The second method uses a Monte-Carlo sampling method that is sometimes used in conjunction with neural networks. The implementation of either of these methods is not trivial, but having accurate representations of the uncertainties of the calculations is necessary.

In the future, it would also be interesting to study pPb reactions. These have been studied in the past for a small number of PDF sets and nuclear corrections (Adeluyi and Bertulani, 2012), but the inclusion of the additional PDF sets, nuclear corrections, additional vector mesons, and additional energies would provide useful information that could also be used to constrain the PDF sets. In a similar fashion, it would also be interesting to study the photoproduction of heavy quarks. In this work I only considered the production of mesons from bare photons. It has been shown by Adeluyi and Bertulani (2012) that the inclusion of resolved photons can have a sizable contribution to the production cross sections. Therefore, the inclusion of the resolved photon components would further the knowledge gained from this work. Finally, in this work I only separated the coherent and incoherent production of the meson for the J/psi at the lower energy using the MSTW09 leading order PDF. A similar treatment for the additional particles, additional PDF sets, and additional energies is also a worthwhile endeavor. As run 2 at the LHC at CERN continues collecting data at the higher energy scale, there will undoubtedly be additional experimental data that can be used to compare against the theoretical predictions.

REFERENCES

Abbas, E. for the Alice Collaboration. (2013) Charmonium and e^+e^- pair photoproductoin at mid-rapidity in ultra-peripheral Pb-Pb collisions at $\sqrt{s_{NN}} = 2.76$ TeV. *The European Physical Journal C,* 73:2617

Adeola, A., and Bertulani, C, (2011). Gluon distribution in nuclei probed at the CERN Large Hadron Collider. *Physics Review C, 84.*

Adeola, A., and Bertulani, C. (2012). Constraining Gluon Shadowing Using Photoproduction in Ultraperipheral pA and AA Collisions. *Physics Review C, 86.*

Altarelli, G., & Parisi, G. (1977). Asymptotic freedom in parton language. *Nuclear Physics B*, *126*(2), 298-318.

Andrade-II, E., González, I., Deppman, A., & Bertulani, C. A. (2015). Evidence of sub-nucleonic degrees of freedom in J/ψ photoproduction in ultraperipheral collisions at the CERN Large Hadron Collider. *Physical Review C, 92*.

Baltz, A.J., Baur, G., d'Enterria, D., Frankfurt, L., Gelis, L., Guzey, V., … Zhalov, M. (2008). The physics of ultraperipheral collisions at LCH. *Physics Reports, 458(1)*, 1-171.

Bertulani, C., and Baur, G., Electromagnetic processes in relativistic heavy ion collisions. *Physics Reports 163.*

Bertulani, C. A., Klein, S. R., & Nystrand, J. (2005). Physics of ultra-peripheral nuclear collisions. *Annual Review of Nuclear and Parcile Science 55*.

Bertulani, C.A., Nathan, A.M. (1993). Excitation and photon decay of giant resonances from high-energy collisions of heavy ions. *Nuclear Physics A 554*, 158-172.

Bertulani, C. A. (2007). *Nuclear physics in a nutshell*. Princeton University Press.

Bettini, A. (2008). *Introduction to elementary particle physics*. Cambridge University Press.

CMS Collaboration. (2012). Suppression of non-prompt J/ψ, prompt J/ψ, and Υ(1S) in PbPb collisions at $\sqrt{s_{NN}} = 2.76$ TeV. *Journal of High Energy Physics 05*, 063.

Das, A., & Ferbel, T. (2003). *Introduction to nuclear and particle physics* (2nd Ed.). World Scientific.

de Florian, D., and Sassot, R. (2004). Nuclear parton distributions at next to leading order. *Physical Review D, 69.*

Deppman, A., Duarte, S. B., Silva, G., Tavares, O. A. P., Anéfalos, S., Arruda-Neto, J. D. T., & Rodrigues, T. E. (2004). The CRISP package for intermediate-and high-energy photonuclear reactions. *Journal of Physics G: Nuclear and Particle Physics*, *30*(12), 1991.

Deppman, A., Tavares, O. A. P., Duarte, S. B., de Oliveira, E. C., Arruda-Neto, J. D. T., de Pina, S. R., ... & Gonçalves, M. (2002). The MCEF code for nuclear evaporation and fission calculations. *Computer physics communications*, *145*(3), 385-394.

Dokshitzer, Y. L. (1977). Calculation of the structure functions for deep inelastic scattering and e+ e− annihilation by perturbation theory in quantum chromodynamics. *Journal of Experimental and Theoretical Physics*, *73*, 1216.

Dulat, S., Hou, T., Gao, J., Guzze, M., Huston, J., Nadolsky, P., Pumplin, J., Schmids, C., Stump. D., & Yuan, C.P. (2015). The CT14 Global Analysis of Quantum Chromodynamics. *arXiv preprint arXiv:1506.07443*.

Eskola, K., Paukkunen, H., and Salgado, C. (2008). An improved global analysis of nuclear parton distribution function including RHIC data. *Journal of High Energy Physics, 102*.

Eskola, K., Paukkunen, H., and Salgado, C., (2009). EPS09-A new generation of NLO and LO nuclear parton distribution functions. *Journal of High Energy Physics, 065.*

Fermi, E. (1924). On the Theory of Collisions between Atoms and Electrically Charged Particles Appeared in Nuovo Cimento 2, pp. 143-158 (1925) (translated from Italian by Michele Gallinaro and Sebastian White, New York 2001).

Gao, J., Nadolsky, P. (2014). A meta-analysis of parton distribution functions. *arXiv preprint arXiv:1401.0013v3*.

González, I., Guzmán, F., & Deppman, A. (2014). Nuclear photoproduction of vector mesons within a Monte Carlo approach. *Physical Review C*, *89*.

Gottfried K., Weisskopf V.F. (1986). *Concepts of particle physics,* (Vol 1). Oxford University Press, USA.

Gribov, V. N., & Lipatov, L. N. (1972). *DEEP INELASTIC ep-SCATTERING IN A PERTURBATION THEORY*. Institute of Nuclear Physics, Leningrad.

Griffiths, D. (2008) *Introduction to Elementary Particles*. John Wiley & Sons.

Halliday, D., Resnick, R., & Walker, J. (2011). *Fundamentals of physics* (extended 9th Ed.). John Wiley & Sons.

Hirai, M., Kumano, S., Nagai, T. (2004). Nuclear parton distribution functions and their uncertainties. *Physical Review ,. 70.*

Kovařík, K., Kusina, A., Ježo, T., Clark., D., Keppel, C., Lyonet, F., Morfín, J., Olness, F., Owens, J., Schienbein, I., and Yu, J. (2015). nCTEQ15-Global analysis of nuclear parton distributions with uncertainties in the CTEQ framework. *arXiv preprint arXiv:1509.00792v1*.

Krane, K. S. (1987). *Introductory nuclear physics*. John Wiley & Sons.

Martin, A.D., Stirling, W.J., Thorne, R.S., & Watt, G. (2009). Parton Distributions for the LHC. *The European Physical Journal C, 63,* 189-285.

Mayer, C. for the ALICE Collaboration, (2014). Coherent photo-production of ρ^0 mesons in ultra-peripheral Pb-Pb collisions at the LCH measured by ALICE. *European Physics Journal Web of Conferences 81*, 02011.

Owens, J.F., Accardi, A., & Melnitchouk, W. (2013). Global parton distributions with nuclear and finite-Q^2 corrections. *Physical Review D 87.*

Povh, B., Lavelle, M., Rith, K., Scholz, C., & Zetsche, F. (2008). *Particles and nuclei: an introduction to the physical concepts*. Springer Science & Business Media.

Rodrigues, T. E., Arruda-Neto, J. D. T., Deppman, A., Likhachev, V. P., Mesa, J., Garcia, C., ... & Tavares, O. A. P. (2004). Photonuclear reactions at intermediate energies investigated via the Monte Carlo multicollisional intranuclear cascade model. *Physical Review C*, *69*.

Thomas, A. W., & Weise, W. (2001). *The structure of the nucleon*. John Wiley & Sons.

Weizsacker, C. V. (1934). Ausstrahlung bei Stößen sehr schneller Elektronen.*Zeitschrift für Physik*, *88*(9-10), 612-625.

Williams, E. J. (1934). Nature of the high energy particles of penetrating radiation and status of ionization and radiation formulae. *Physical Review*, *45*(10), 729.

Wong, S. S. (1998). *Introductory nuclear physics* (2nd Ed.). John Wiley & Sons.

Zhu, S. (2003). Understanding Pentaquark States in QCD. *Physical Review Letters. 91(23).*

VITA

After graduating from Canyon High school in 2006, James O. Thomas enrolled at West Texas A&M. He received a Bachelor of Science degree with a major in physics and a minor in mathematics in May of 2014. Before enrolling in the graduate school of Texas A&M University-Commerce, he participated in a summer internship at Sandia National Lab in Albuquerque New Mexico. He was enrolled in the graduate school of Texas A&M University-Commerce in August of 2014. While there he received many awards, including Outstanding Graduate Student and being named a fellow of the NASA/Texas Space Grant Consortium for the 2015/2016 academic year. He was awarded the Master of Science degree in May of 2016.

Permanent address:
James O. Thomas
Department of Physics and Astronomy
Texas A&M University-Commerce
P.O. Box 3011
Email: jamesothomas@gmail.com